TAL
TECH
SCHOOL OF
SCIENCE

Controlling Drug Delivery through Macrophage and Nanoparticle Interactions: An Exploration of Inflammation-Responsive Mechanisms

Master’s thesis

Student: Laura Kaarma
Supervisor: Alexandra Stubelius, PhD, Associate professor
Chalmers University of Technology
Co-supervisor: Kaja Kasemets, PhD, Senior researcher
National Institute of Chemical Physics and Biophysics
Study program: Applied Chemistry and Biotechnology

Tallinn 2023

LOODUSTEADUSKOND

Ravimi edastamine makrofaagide ja nanoosakeste interaktsioonide kaudu: põletikureaktsioonidele reageerivate mehhanismide uurimine

Magistritöö

Üliõpilane: Laura Kaarma
Juhendaja: Alexandra Stubelius, PhD, dotsent
Chalmersi Tehnikaülikool
Kaasjuhendaja: Kaja Kasemets, PhD, vanemteadur
Keemilise ja Bioloogilise Füüsika Instituut
Õppekava: Rakenduskeemia ja biotehnoloogia

Tallinn 2023

Author's declaration and supervisor's resolution

Hereby I declare that I have compiled the paper independently and all works, important standpoints and data by other authors have been properly referenced and the same paper has not been previously been presented for grading.

Author: Laura Kaarma
[Signature, date]

The paper conforms to requirements in force.
Supervisors: Alexandra Stubelius, Kaja Kasemets
[Signature, date]

May 26th 2023

Contents

Abbreviations 6

Introduction 7

1. Literature review 9

  1.1. Rheumatoid arthritis 9

    1.1.1. Pathology 9

    1.1.2. Macrophages and their role in inflammation 10

    1.1.3. Current treatment methods 12

  1.2. Nanoparticle based RA therapy research 13

    1.2.1. Acetalated dextran and phenylboronic pinacol ester dextran nanoparticles as nanocarriers 14

  1.3. NPs in RA 16

  1.4. Aims of the study 17

2. Materials and methods 18

  2.1. Chemicals 18

    2.1.1. Fluorescent probes 19

    2.1.2. Lipopolysaccharide 19

    2.1.2. Ac-Dex and PBE-Dex polymer synthesis 19

    2.1.3. NP synthesis 20

  2.2. Method workflow 20

    2.2.1. Probe characterization 21

    2.2.2. Characterization of NPs 21

    2.2.3. Model drug loading and encapsulation efficiency 21

  2.3. Cell studies 22

    2.3.1. Macrophage cell line 22

    2.3.2. General cell culturing 22

    2.3.3. FDA and DC-FDA titration and time-dependency assays 23

    2.3.4. LPS titration and time-dependency assays 23

    2.3.5. Method development: biological ON/OFF/ON-system 24

    2.3.5. Cytotoxicity assay 24

    2.3.6. Enzyme linked immunosorbent assay 25

  2.4. Statistical analysis 25

3. Results and Discussion 27

3.1. Material characterization ... 27
  3.1.1. Probe characterization ... 27
  3.1.2. Characterization of NPs ... 28
  3.1.3. Model drug loading and encapsulation efficiency ... 29
3.2. Cell studies ... 30
  3.2.1. Pre-testing FDA and DC-FDA concentrations with different LPS doses ... 31
  3.2.2. Optimizing LPS and prednisolone concentrations and time of incubation ... 36
  3.2.3. ELISA ... 39
  3.2.4. Cytotoxicity assay ... 40
  3.2.5. ON/OFF-system ... 41
Abstract ... 43
Annotatsioon ... 44
Acknowledgments ... 45
References ... 46
Appendices ... 53
Appendix 1 Cell splitting protocol ... 53

Abbreviations

Ac-Dex – acetalated dextran

ACPA – anti-citrullinated protein antibodies

Ac/PBE-Dex – 4-(hydroxymethyl)phenylboronic pinacol ester conjugated to acetalated dextran

bDMARDs – biologic DMARDs

CDI – N,N-Carbonyldiimidazole

csDMARDs – conventional synthetic DMARDs

CXCL – chemokine (C-X-C motif) ligand

DDS – drug delivery system

DLS – dynamic light scattering

DC-FDA – 2’,7’-dichlorofluorescein diacetate

DMEM – Dulbecco's Modified Eagle Medium

DMARDs – disease-modifying antirheumatic drugs

HCQ – hydroxychloroquine

ELISA – enzyme linked immunosorbent assay

FDA – fluorescein diacetate

FI – fluorescence intensity

FLS – fibroblast-like synoviocytes

IL – interleukin

ISO – International Organization for Standardization

LEF – leflunomide

LPS – lipopolysaccharide

MDMs – monocyte-derived macrophages

MMP – matrix metalloproteinase

MTX – methotrexate

NP – nanoparticle

NSAIDs – nonsteroidal anti-inflammatory drugs

PBE - phenylboronic pinacol ester

PDI – polydispersity index

PRDL – prednisolone

RA – rheumatoid arthritis

RT – room temperature

ROS – reactive oxygen species

SSZ – sulfasalazine

TNF-α – tumour necrosis factor alpha

tsDMARDs – targeted synthetic DMARDs

λem – emission wavelength (nm)

λex – excitation wavelength (nm)

Introduction

Inflammation is a fundamental physiological response in the body, acting as a protective measure against harmful stimuli such as pathogens, damaged cells, or irritants [1]. It manifests as a complex biological response involving various cellular and molecular mechanisms. However, when inflammation becomes chronic or systemic, it can shift from being a defensive mechanism to a harmful process that contributes to the pathogenesis of numerous diseases, including autoimmune disorders like rheumatoid arthritis (RA). As a shared pathological feature among many diseases, inflammation offers a common therapeutic target [2]. Since inflammation serves as one of the key symptoms and underlying triggers in the pathogenesis of RA, it becomes critical to investigate and understand its complexities for the development of more targeted and effective treatment strategies.

RA is a common autoimmune disease which according to World Health Organization estimates affects around 24 million people globally [3]. It leads to various complications including systemic disorders and progressive joint damage [4]. Despite current treatments such as nonsteroidal anti-inflammatory drugs (NSAIDs), glucocorticoids (GCs), and disease-modifying antirheumatic drugs (DMARDs) [5], many patients continue to require sustained pharmaceutical therapy due to insufficient long-lasting results. In the pursuit of improved treatment options, extensive research has explored the potential of nanotechnology as a viable therapeutic approach for RA. Nanoparticles (NPs) offer a promising strategy by acting as nanocarriers and encapsulating bioactive agents, allowing targeted delivery to the affected areas [6]. This approach offers several advantages, including the ability to maintain therapeutic efficacy without the need to increase drug concentration or frequency of dosing. Furthermore, NPs enhance the solubility of various drugs, preventing their degradation within the body.

The following thesis aimed to delve deeper into this promising field, exploring how nanotechnology could revolutionize the approach to treating RA. The goal was to develop a drug delivery system (DDS) for RA using loaded acetalated dextran (Ac-Dex) and acetalated dextran and 4-(hydroxymethyl)phenylboronic pinacol ester conjugated to dextran (Ac/PBE-Dex) NPs and Raw 264.7 macrophages to control the release of a model drug. By activating macrophages with bacterial lipopolysaccharide (LPS), an environment similar to inflammation was created (referred to as the ON-state) characterized by a lower pH compared to healthy conditions. The NPs used were previously determined to be pH sensitive and would ideally degrade and release their cargo upon entering the inflamed microenvironment. To demonstrate the particles' specificity, the glucocorticoid drug prednisolone was introduced to cells to restore their healthy condition (OFF-state). The model drug used was a probe which was metabolically converted by cells into a fluorescent component. The resulting signal and changes in fluorescence intensity (FI) were captured using a microplate reader.

The work process was divided into two parts; the first half consisted of material and probe characterisation, including NP size and stability because NP behaviour is influenced by their properties. This provided insight into how the NPs would react in an inflamed environment. The second part entailed the model development, more specifically cell studies to confirm the optimal concentrations for the fluorescent probes, LPS and NPs. A viability assay based on cell metabolism was used to determine NP biocompatibility. To verify cell activation, the level of the pro-inflammatory cytokine interleukin-6 (IL-6) was measured through an enzyme-linked immunosorbent assay (ELISA) confirming high levels of IL-6 in LPS stimulated cells compared to unstimulated cells. Finally, the assays were combined to achieve a highly sensitive, biologically controlled ON/OFF drug release system.

This study highlighted the potential of a self-regulating DDS employing loaded NPs to offer a controlled treatment for RA patients. By mitigating adverse side effects, managing disease aggravation, and addressing systemic impacts, this innovative approach could represent a promising alternative to conventional RA therapies.

1. Literature review

1.1. Rheumatoid arthritis

RA is a widely spread autoimmune disease affecting 0,4% to 1,3% of the population [7]. It has two to three times higher prevalence in women than in men, higher frequency in the 60+ age group and in urban areas. RA is one of the most common chronic inflammatory diseases causing synovial inflammation and hyperplasia ("swelling"), autoantibody production, cartilage and bone destruction, cardiovascular, pulmonary, psychological and skeletal disorders [4]. It is classified as an inflammatory type of arthritis as opposed to the non-inflammatory type known as osteoarthritis [8]. It is presumed that RA is caused by the dysregulated citrullination which leads to the production of anti-citrullinated protein antibodies (ACPAs) but the exact molecular mechanisms remain unknown [9]. According to previous studies on adults in the United States, arthritis is the most common medical cause of mobility-related functionality loss which makes it a public health issue [10]. It has also been shown that reducing the risk factors of RA or treating recently diagnosed cases has a lower economic impact than treatment methods applied in the later stages of the disease [11].

1.1.1. Pathology

Although RA etiology remains unclear, the changes in the synovium and synovial fluid are known [12]: macrophages start producing cytokines which stimulate fibroblast-like synoviocytes (FLS), a specialized type of synovial cells which can migrate between joints for example in the hands, and increase the activity of the bone degrading cells osteoclasts [13] which leads to bone erosion. At the same time cartilage degradation occurs because of FLS produced matrix metalloproteinases [14]. The migration of FLS creates a pattern described as symmetrical RA [15]. Furthermore, FLS increases the expression of nuclear factor-kB ligand receptor activator leading to T cell binding proteins on the surface of osteoclasts and ultimately bone erosion [16]. Along with promoting bone erosion, CD4+ T cells also promote the secretion of interleukin 17, a cytokine which stimulates synovial macrophages and FLS and thus starting the inflammatory process [17].

Besides FLS, T cells and macrophages, neutrophils, antibodies and the forming of new blood vessels have been found in the synovial fluid. Neutrophils produce proteases and reactive oxygen species (ROS) which further aggravate bone erosion and cartilage degradation [18]. Antibodies over-activate the immune system and promote inflammation by binding to each other [19]. Angiogenesis, a process where new blood vessels are formed from existing ones, is one of the major elements in RA because it facilitates the migration of immune cells into joints [20]. The proangiogenic factor vascular endothelial growth factor has been linked to bone destruction by promoting the formation of osteoclasts [20]. Figure 1 summarises the pathophysiological processes that result in the appearance of symptoms in RA.

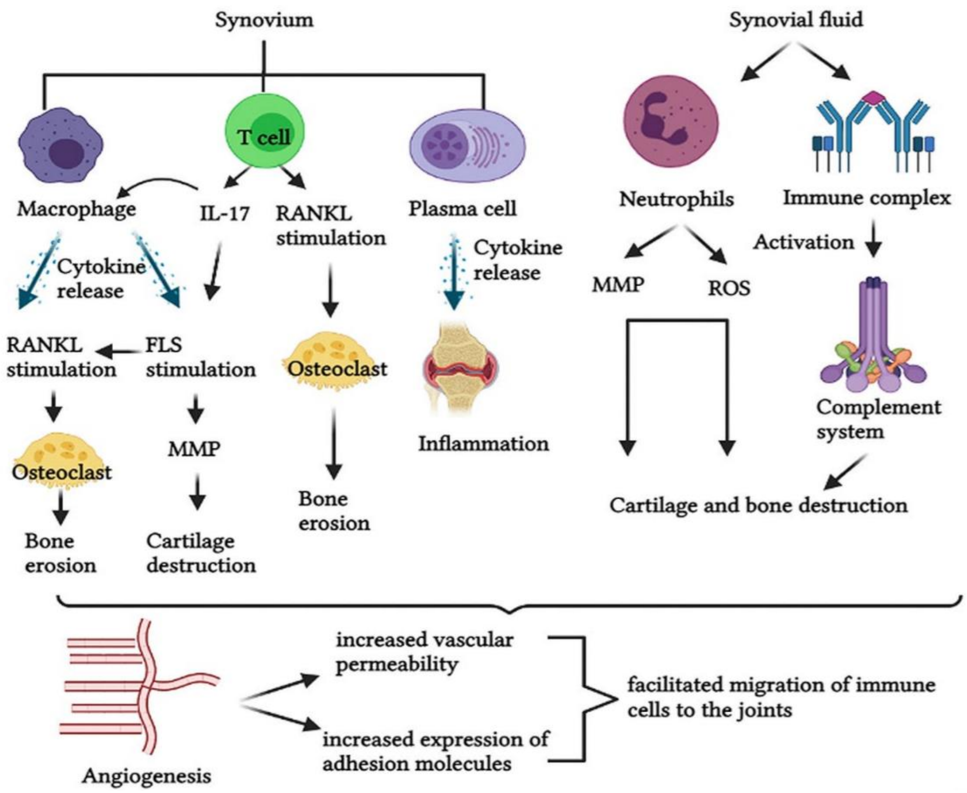
Synovium
Synovial fluid
T cell
Macrophage
IL-17
RANKL stimulation
Plasma cell
Neutrophils
Immune complex
Cytokine release
Cytokine release
Activation
MMP
ROS
RANKL stimulation
FLS stimulation
Osteoclast
Osteoclast
MMP
Inflammation
Complement system
Bone erosion
Cartilage destruction
Bone erosion
Cartilage and bone destruction
Angiogenesis
increased vascular permeability
increased expression of adhesion molecules
facilitated migration of immune cells to the joints

Figure 1. Pathological mechanisms in RA. IL – interleukin; FLS – fibroblast-like synoviocytes; MMP – matrix metalloproteinase; RANKL – receptor activator of nuclear factor-kB ligand; ROS – reactive oxygen species. Figure adapted from Radu et al. [8]

1.1.2. Macrophages and their role in inflammation

Macrophages are a group of immune cells specialized in the detection, phagocytosis and destruction of harmful organisms e.g. bacteria, viruses or dead cells in our body. They also produce antigens to recruit T cells and initiate inflammation by releasing cytokines, a class of small proteins, which serve as a signal for other cells to activate. Macrophages are either derived from tissue or differentiated from blood monocytes and their populations are highly heterogenous. In addition to cytokines, they release ROS which help in the destruction of phagocytosed bacteria. Macrophages are found in most tissues taking on different forms such as microglia in the central nervous system or Kupffer cells in the liver [21]. In response to the changes in their surrounding environment, the cells polarize to M1 or M2 subtypes [22]: M1 macrophages are capable of pro-inflammatory responses and secrete cytokines such as IL-6, IL-10 and tumor necrosis factor alpha (TNF-α) [23] whereas the M2 subtype produce anti-inflammatory responses and mend damaged tissue [24]. Should an infection occur, macrophages first polarize to the M1 phenotype and later to M2 to help clear the damage and restore the tissue.

In the case of RA, macrophages are responsible for driving both inflammation and chronicity within the joint. They secrete a number of factors closely linked to the disease, including pro-inflammatory cytokines like TNF-α, IL-1 and IL-6, chemoattractants like CCL2 and IL-8, as well as tissue remodelling enzymes like MMP-3 and MMP-12 [25]. The development of a hypertrophic synovial lining layer in RA patients is attributed to fibroblast proliferation, increased vasculature, and the infiltration of monocyte-derived macrophages (MDMs) from the circulation. Monocyte recruitment is directly linked to the degree of synovitis, leading to an increase in the total synovial macrophage population [26]. The total synovial macrophage population increase is directly related to disease activity, and it is employed as a biomarker to assess the efficacy of different treatments [27]. These findings have been studied through a variety of mouse models of RA [28]. Studies in humans with radiolabelled CD14+ monocytes have shown that monocytes actively migrate to the inflamed joint, where they polarize to inflammatory MDMs in the inflamed synovium [29]. The presence of distinct disease activity subtypes depending on the cellular infiltrate can be identified through histological analysis, which can be used to define synovitis [30].

The synovial lining in RA patients becomes hypertrophic, leading to reduced oxygen levels in the joint that can drop to less than 1% [31]. This environment causes changes in macrophage respiration and promotes pro-inflammatory activation through upregulation of hypoxia-inducible factor 1-alpha, resulting in anaerobic glycolysis and reduced oxidative phosphorylation [32]. Myeloid-specific deletion of hypoxia-inducible factor 1-alpha has been shown to reduce inflammation and joint swelling in murine models of arthritis [33]. Two populations of pro-inflammatory monocytes have been identified in RA models, including classical Ly6C+ monocytes that drive inflammation in adjuvant and antigen-induced arthritis, and non-classical Ly6C- cells that recruit in sterile models of autoantibody-induced arthritis [34]. The activated macrophages can change their polarization from a pro-inflammatory M1 type to a non-classical M2 anti-inflammatory phenotype, which is necessary for inflammation resolution [35] and the conversion of pro-inflammatory macrophages to a pro-resolution phenotype may be a viable therapeutic strategy for human disease. The role of macrophages in inflammation is summarized in Figure 2.

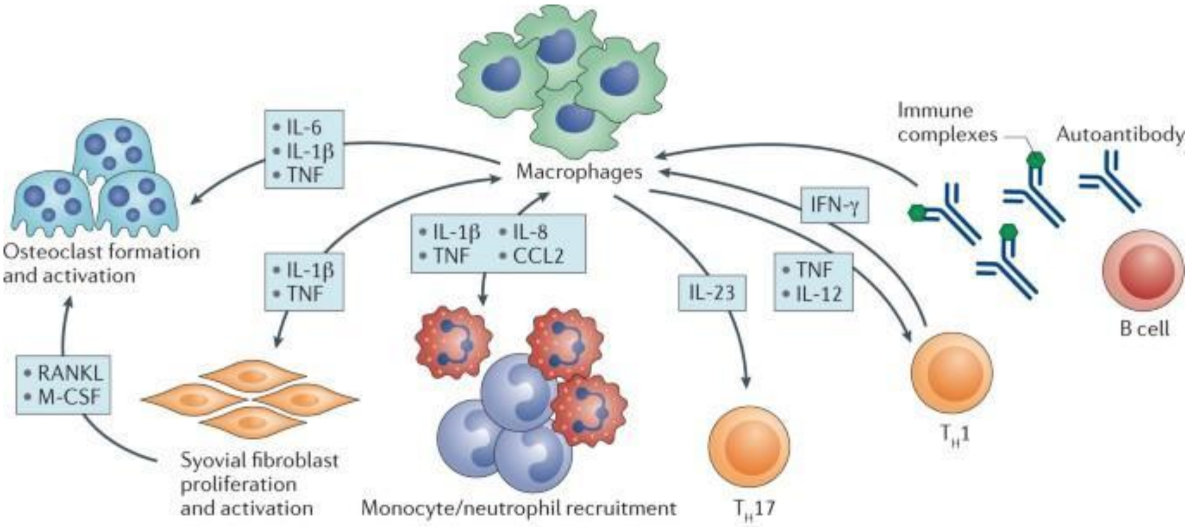

Figure 2. Macrophage role in inflammation. Macrophages play a critical role in RA by promoting Th1 and Th17 cell activation, B cell differentiation and antibody production, and the recruitment of monocytes and neutrophils to the synovium. They also contribute to synovial fibroblast proliferation and activation, osteoclast activation and formation, and the production of pro-inflammatory cytokines, which exacerbate disease pathology. Figure adapted from Udalova et al. [35]

Distinct subsets of macrophages in the synovium have been identified through early histological studies of inflamed patient tissue, depending on combinations of individual antibody clones used for labelling [36]. These subsets change in frequency based on the levels of disease activity observed in the tissue. In active disease, pro-inflammatory MDMs make up the majority of synovial macrophages [30], and they are capable of releasing pro-inflammatory mediators like TNF, IL-1, IL-6, chemokine (C-X-C motif) ligand 8 (CXCL8), and chemokine (C-C motif) ligand 2 when isolated from inflamed tissues of RA patients with active disease [37]. Additionally, these macrophages are able to stimulate autologous T cells [39]. It is widely recognized that RA MDMs exhibit a pro-inflammatory profile, characterized by the secretion of CXCL4 and CXCL7 that promote the migration of neutrophils and monocytes to the inflamed joint [37], as well as the release of other cytokines [38]. MDMs in the synovium can be identified with an antibody against an epitope on the alarmins S100A8/9 [39], and they are susceptible to anti-TNF therapy, leading to their rapid removal [40]. Interestingly, synovial lining macrophages are not responsive to anti-TNF treatment, which suggests that selectively targeting MDMs could be a therapeutic approach.

1.1.3. Current treatment methods

Due to the unknown nature of the molecular mechanisms of RA, currently existing treatments do not offer a fast recovery. In order for therapeutic intervention to have a positive effect, it must be aggressive and rapid since the damage to joints is non-reversible [41]. The best therapeutic approaches are early diagnosis along with physiotherapy, conventional synthetic DMARDs (csDMARDs), biologic DMARDs (bDMARDs) and targeted synthetic DMARDs (tsDMARDs) [42]. NSAIDs and GCs are used as primary and secondary inflammation reducing agents to relieve the symptoms [43].

The pharmacological treatments are able to alleviate the symptoms and inhibit the progression of RA. They are divided into symptomatic treatment and disease modifying treatment [44]. The former includes mainly NSAIDs and GCs with weak opioid analgesics as a temporary solution to reduce pain [45]. NSAIDs decrease inflammation by blocking the action of cyclooxygenase, mainly cyclooxygenase-2 (COX-2), which produce the chemical messengers prostaglandins, and are taken in the acute phase response of RA as pain relievers [46]. Examples of widely used NSAIDs in RA include ibuprofen, coxibs and naproxen. On the other hand, this can lead to severe side effects for example bleeding, heart failure, seizures, gastrointestinal ulceration, etc. More specific forms of NSAIDs (celecoxib, rofecoxib, valdecoxib) that are selective towards COX-2 have been developed to avoid some of the risks [47].

NSAIDs are frequently used for symptomatic relief of inflammatory conditions, including RA, osteoarthritis, and juvenile RA, despite their inability to reduce acute-phase reactants or alter radiographic progression [47]. Their efficacy is largely attributed to the inhibition of prostaglandin production in peripheral tissues and the central nervous system, involving both cyclooxygenase-1 (COX-1) and COX-2 in the nociception process [48]. However, NSAIDs can cause renal, hepatic, and cardiovascular side effects [49]. Sodium retention, potentially leading to weight gain, peripheral edema, and congestive heart failure can occur, especially in patients with mild heart failure or liver disease. Increases in one or more liver tests have been reported in up to 15% of patients, with significant elevations in some cases, potentially leading to rare but severe outcomes. Diclofenac and sulindac have been most associated with hepatic adverse events. Additionally, the introduction of COX-2-selective NSAIDs revealed cardiovascular risks tied to NSAID use, with COX-2 inhibitors such as rofecoxib causing increased risk of myocardial infarction and stroke, leading to its withdrawal from the market [50]. The cardiovascular risk with NSAIDs is thought to be related to the degree of COX-2 inhibition and incomplete COX-1 inhibition [51].

While GCs are more potent than NSAIDs, they cause further side effects like weight gain and diabetes, limiting their use to brief periods for inflammation and immune response control [52]. European databases reveal that half of RA patients receive prolonged, low-dose GC therapy, with its efficacy-to-adverse-event ratio being favourable day [52]. Interestingly, GC therapy has in some cases significantly slowed erosion progression in RA patients, an effect that persisted even after stopping the treatment, suggesting an impact beyond their anti-inflammatory function [53]. However, GC's associated adverse events need to be considered in relation to the chronic inflammation they're treating, which increases comorbidity risks such as cardiovascular diseases and inflammatory bone loss. The potential of GCs in reducing these risks may offset their negative effects, as demonstrated by comparable blood glucose and C-peptide levels between RA patients under longstanding GC treatment and GC-naïve patients.

Although low-dose GCs are associated with adverse events, these must be evaluated in the context of the treated inflammatory condition. Chronic inflammation increases the risk of comorbidities such as cardiovascular diseases, infections, insulin-resistance, and inflammatory bone loss. Thus, reducing these risks by reducing chronic inflammation may counterbalance the negative effects of GCs [52]. For example, patients with RA showed an increased area under the curve of blood glucose as well as C-peptide compared to healthy controls, but no difference was observed between RA patients on longstanding GC treatment and those who were GC-naïve [54].

DMARDs are drugs used for disease-modifying treatment in RA to suppress autoimmune activity and protect joints. They are divided into csDMARDs, bDMARDs and tsDMARDs [42]. csDMARDs such as methotrexate (MTX), leflunomide (LEF), hydroxychloroquine (HCQ), and sulfasalazine (SSZ) are used in early cases due to their lower efficacy but fewer adverse reactions [55]. According to the 2021 guideline of the American College of Rheumatology, MTX is the preferred drug for first-line treatment whether as a monotherapy or in conjunction with other drugs because of its efficacy, safety profile, ease of administration and low cost [56]. Alternatives to MTX include LEF, HCQ, and SSZ, and the suggested order of drugs for patients who have never received DMARD treatment and have a low disease activity is HCQ, SSZ, MTX, and LEF.

1.2. Nanoparticle based RA therapy research

While NSAIDs, DMARDs, GCs and other biological agents enable relief of RA symptoms through immunosuppression or inhibiting inflammatory agents, they do not offer a permanent solution to the disease. The body has multiple physiological barriers that the drugs need to overcome: for example, in the blood stream the phagocytose of reticuloendothelial-system and the destruction of proteases pose a serious challenge. Current pharmacological treatments cannot make changes to the pathological mechanisms, they have reduced bioavailability, uneven distribution which reduces their therapeutic efficacy and often causes adverse effects. Thus, their usage must be limited to shorter periods and lower doses. These issues have led to research on nanomedicines in RA treatment.

One promising approach are nanocarriers – drug delivery systems consisting of 1-500 nm sized particles with a drug or bioactive agent inside the NP. Their physicochemical properties are easily controlled, they can increase the solubility and circulation time of drugs and allow a controlled delivery to the targeted area [57]. The materials that have been used for nanocarriers are biocompatible and biodegradable such as polymers, lipids, gelatin, albumin or polysaccharides [58]. For small molecule drug delivery, effective nanocarriers should encapsulate the drugs with high drug loading while preventing drug leakage and release prior to reaching inflamed sites. To address these challenges, multifaceted delivery strategies can be divided into two main categories: conjugating drugs with NPs and encapsulating drugs within NPs [59]. Harnessing the potential of NPs for targeted drug delivery requires a deep understanding of the factors that influence the various properties NPs.

The size of NPs is greatly influenced by various process parameters such as the amount of drug or polymer, the drug-polymer ratio, the ratio of solvent to anti-solvent, stirring time, and reaction temperature [60]. Higher viscosity of the organic solvent, higher polymer concentration, and slower flow rate prolong the mixing time, leading to an increase in particle size and PDI [61]. On the other hand, although larger NPs are produced with a higher amount of polymer, they generally exhibit better drug encapsulation efficiencies compared to the smaller particles. Studies have indicated that higher drug concentrations lead to a greater number of nuclei at the interface between the solvent and anti-solvent causing the aggregation and formation of larger NPs [62]. Additionally, an increase in viscosity caused by higher drug concentrations hampers the diffusion of the drug from the solvent to the anti-solvent, consequently reducing the yield of NPs [63].

Solvents with high diffusion rates, such as acetone and acetonitrile, have been observed to promote the formation of smaller NPs with narrower size distributions [64]. The use of solvents with low boiling points is also desirable as it facilitates the evaporation process and the formation of the particles. Several researchers have reported that the ratio of solvent to anti-solvent plays a significant role. It has been observed that an increase in the proportion of anti-solvent relative to solvent (in the range of 1:2 to 1:20) leads to the production of smaller NPs. In general, higher stirring rates have been found to result in the production of smaller NPs [65]. For example, an increase in the stirring rate from 300 to 1200 rpm led to a reduction in particle size from 800 to 300 nm [62]. This decrease in particle size can be attributed to improved mass transfer and diffusion rates, which facilitate rapid nucleation and precipitation. A decrease in temperature from 40 to 10 °C resulted in a reduction in particle size from approximately 800 to 300 nm, as observed by Zhang et al [62]. They proposed that the lower solubility at lower temperatures leads to higher supersaturation and a faster nucleating rate.

1.2.1. Acetalated dextran and phenylboronic pinacol ester dextran nanoparticles as nanocarriers

The aim of this thesis was to use NPs consisting of two modified dextran polymers for drug delivery. The first modification involved acetalation of dextran, resulting in pH sensitivity of the polymer, referred to as Ac-Dex. The second modification involved phenylboronic pinacol ester modification of dextran, enabling the generation of ROS sensitivity. Two types of NPs were tested for the

ON/OFF/ON-system: ones consisted of Ac-Dex and the others of both Ac-Dex and PBE-Dex (Ac/PBE-Dex NPs).

Ac-Dex is one of the most investigated chemically modified derivatives of the polysaccharide dextran, a polymer which has been approved by the Food and Drug Administration for use in medicine [66]. It is biodegradable, sensitive towards environments with acidic pH for example an inflamed area, has a high encapsulation efficacy with certain NPs and can cross the mucosal barrier. The synthesis of Ac-Dex is achieved through the catalysation of dextran and 2-methoxypropene by pyridinium p-toluenesulfonate. It is insoluble in water due to the acetalation of pendant hydroxyl groups but can be dissolved in organic solvents such as ethanol, ethyl acetate and dichloromethane [67]. In addition, the acetal groups in acetalated dextran are susceptible to acidic hydrolysis, resulting in the recovery of dextran as well as methanol and acetone as degradation by-products. Because of its hydrophobic properties and solubility, a drug can be encapsulated within NPs consisting of Ac-Dex either by precipitation or emulsion and later released by acid-triggered degradation [68]. Over the past decade, there has been an increasing interest in Ac-Dex-based drug delivery systems such as vaccines due to its relatively simple preparation, fabrication, and controllable degradation.

Ac-Dex contains both cyclic and acyclic acetal groups, with the formation of acyclic acetals being kinetically favoured and occurring rapidly (Figure 3). Within 5 minutes, more than 80% of hydroxyl groups can be substituted by acyclic acetals, as indicated by detailed kinetic studies [69]. In contrast, the formation of cyclic acetals is thermodynamically favoured, and with prolonged reaction time, cyclic acetals gradually replace acyclic ones. By adjusting the reaction time, Ac-Dex with varying ratios of cyclic and acyclic acetals can be acquired which is an important structural characteristic as it directly affects the polymer's degradation rate. Acyclic acetals hydrolyze rapidly into methanol and acetone, while cyclic acetals slowly hydrolyze into acetone. Thus, by controlling the ratio of cyclic and acyclic acetals, the polymer's degradation half-life can be regulated [70]. The Ac-Dex NPs used in the current thesis had 35% of their hydroxyl groups involved in cyclic acetalization.

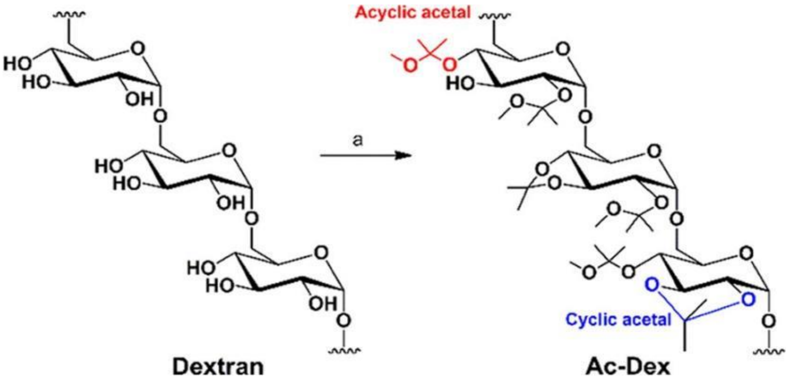

Figure 3. Cyclic and acyclic structure of Ac-Dex. Figure adapted and modified from Broaders et al. [70]

By varying the conjugation group, different sensitivities can be achieved for PBE-Dex moieties. Their responsiveness to ROS species can be affected through conjugating their hydroxy group (4-(hydroxymethyl) phenylboronic pinacol ester), carboxy group (4-(carboxymethyl)phenylboronic pinacol ester), or any other group (such as amino-groups) (Figure 4). This sensitivity modulation is based on the hydrolysis of boronic pinacol ester into boronic acid and pinacol. Additionally, a quinone methide rearrangement occurs, which relies on the linkage between the phenylboronic pinacol ester and the polymer. As a result, the hydrophilic characteristics of dextran are restored [71]. It is important to note that ROS species are consumed during this process, giving the polymer scavenging properties.

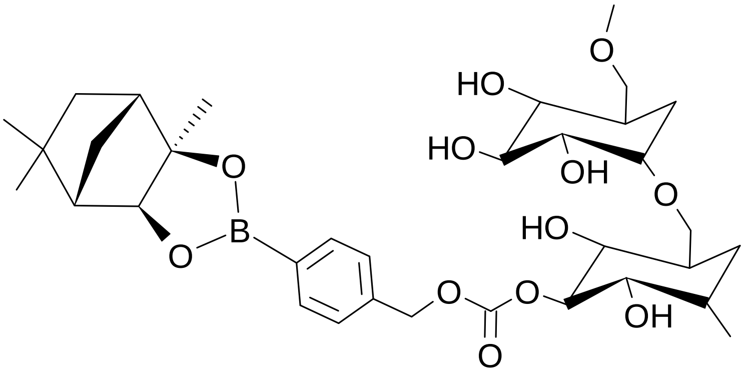

Figure 4. Chemical structure of modified dextran with 4-(methyl hydroxy) boronic acid pinacol ester. Figure adapted from Manaster et al. [72]

1.3. NPs in RA

The development of nanomedicine for treating RA has recently surged to overcome the limitations of current treatments. Abnormal vessels and inflammatory cell infiltration in RA sites lead to improved vascular permeability, allowing for passive accumulation of NPs through the "ELVIS" effect (extravasation through leaky vasculature and subsequent inflammatory cell-mediated sequestration) [73]. This effect is similar to the enhanced permeability and retention effect observed in solid tumours and has been shown to effectively deliver various drugs into RA sites, leading to enhanced drug accumulation and reduced side effects [73]. Additionally, actively targeting DDS have been designed by modifying specific recognition ligands on the surface of NPs, taking advantage of the overexpression of certain receptors on inflammation-associated cells. Particle size plays a crucial role in developing a passive targeting method, where NPs conjugated with drugs between 100 to 200 nm can avoid removal by the mononuclear phagocyte system and reticuloendothelial system, leading to extended blood circulation in RA patients [74]. Various NP modifications can further improve passive drug delivery and reduce off-target effects. However, despite significant progress, the field of nanomedicine for RA management is still in its early stages, and there is a lack of effective treatments.

Active drug delivery involves communication between therapeutic agents, NPs, and target cells, often facilitated by ligand-receptor interactions [75]. These interactions require direct contact between the ligand and receptor [76], and the carrier system is modified with functionalized surfaces to avoid biological uptake by the reticuloendothelial system and to transport the drug to the target location. Various surface coatings, including biological bonding agents, non-ionic surfactants, specific cells or antibodies, and albumin protein, can improve the specificity of drug delivery [77]. Figure 5 depicts the different types of NPs used for drug delivery.

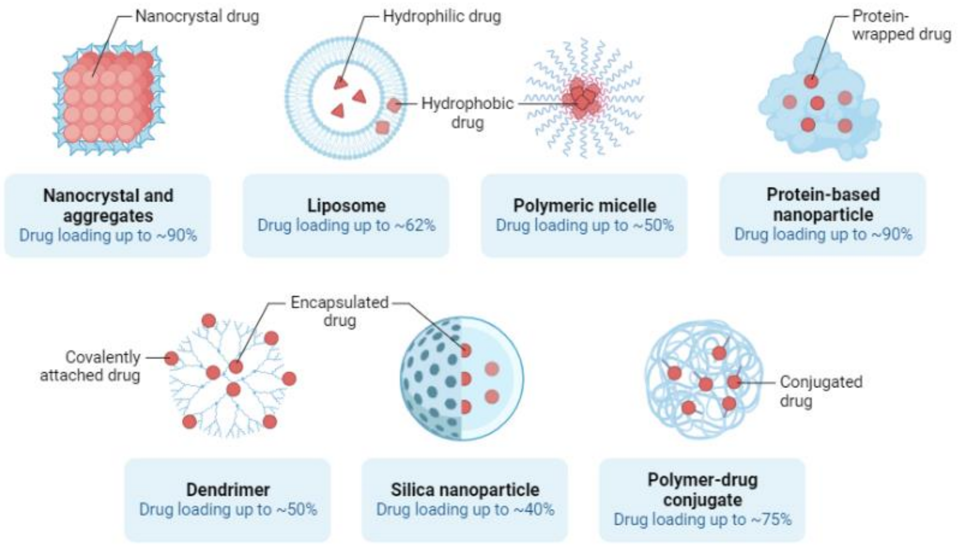
Nanocrystal drug
Hydrophilic drug
Hydrophobic drug
Protein-wrapped drug
Nanocrystal and aggregates
Drug loading up to ~90%
Liposome
Drug loading up to ~62%
Polymeric micelle
Drug loading up to ~50%
Protein-based nanoparticle
Drug loading up to ~90%
Encapsulated drug
Covalently attached drug
Conjugated drug
Dendrimer
Drug loading up to ~50%
Silica nanoparticle
Drug loading up to ~40%
Polymer-drug conjugate
Drug loading up to ~75%

Figure 5. Nanoscale delivery approaches for small-molecule cargoes. Retrieved from BioRender.com (2023). [78]

To enhance the accumulation of NPs in inflamed joints, active targeting approaches have been developed, which involve modifying the surface of nanodrugs with location-targeting ligand molecules. This surface alteration enables the NPs to be internalized more efficiently by the elevated membrane receptors or surface protein levels present on RA-affected cells, thus aiding their entry into the cells. Once the drug-loaded NPs reach the targeted tissue, they may act at the cytosolic level or within the cytomembrane [79]. The drug may be released from the vehicle on the cell surface, in the extracellular matrix, or through lysosomal organelles' lytic and digestive enzymes. This mechanism ensures the discharge of the drug into the cytosol without the colloidal carrier moiety's attachment [80].

1.4. Aims of the study

The primary objective of this thesis was to develop a NP-based DDS that aligns with the severity of inflammation and can be regulated through the biochemistry of inflammation, including factors like pH and ROS. The NPs used were loaded with two fluorescent probes which acted as a model drug. The probes were used instead of a drug to more specifically investigate the particle release properties. Additionally, this system would be controlled via an innovative ON/OFF/ON mechanism, which could potentially minimize drug-induced side effects. This strategy stems from the observation that during an inflammatory response, specifically within joints, the pH level decreases from the norm due to heightened metabolic activity in macrophages [86]. These characteristic changes in the pH level provide a unique opportunity to control drug. The fluctuating pH during inflammation acts as a trigger, enhancing the specificity and efficiency of therapies and minimizing side effects.

This method presents a new frontier in the realm of personalized medicine, as the DDS would tailor the delivery and dosage of drugs based on individual patient's inflammatory response. Not only would this revolutionize the way drugs are administered, but it could also lead to better patient outcomes, improved drug efficacy, and a lower incidence of adverse effects.

2. Materials and methods

2.1. Chemicals

All chemicals and compounds used in this thesis are listed in Table 1.

Table 1. CAS-numbers and manufacturers of chemicals used in experiments.

Chemical	CAS-number	Manufacturer
2’,7’-dichlorofluorescein diacetate	2044-85-1	Sigma Aldrich Sweden AB
2-methoxypropene	116-11-0	Acros Organics
4-(Hydroxymethyl)phenylboronic acid pinacol ester	302348-51-2	Sigma-Aldrich
Acetalated dextran	-	Gizem Erensoy
Acetone (HPLC grade)	67-64-1	Fisher Scientific
D-(+)-Trehalose dihydrate	6138-23-4	Alfa Aesar
Dextran (from *Leuconostoc mesenteroides*, 9-11 kDa)	9004-54-0	Sigma Aldrich
Dichloromethane	75-09-2	Sigma-Aldrich
Dimethyl sulfoxide	2206-27-1	Sigma-Aldrich
Dulbecco´s Modified Eagle´s Medium	-	Thermo Fisher Scientific (Gibco)
Erythrosin B	15905-32-5	Sigma-Aldrich
Fetal bovine serum (FBS)	-	Thermo Fisher Scientific (Gibco)
Fluorescein diacetate	596-09-8	Sigma-Aldrich Sweden AB
Lipopolysaccharide	93572-42-0	Sigma-Aldrich
N,N-Carbonyldiimidazole	530-62-1	Sigma-Aldrich
N,N-Dimethylformamide	68-12-2	Alfa Aesar
Phosphate buffered saline (with calcium and magnesium)	-	Thermo Fisher Scientific (Gibco)
Prednisolone	50-24-8	Sigma Aldrich Sweden AB
Pyridinium p-toluensulphate	24057-28-1	Acros Organics
Resazurin	62758-13-8	Alfa Aesar
Sodium hydroxide	1310-73-2	Fisher Scientific
Sulfuric acid	7664-93-9	Sigma-Aldrich Sweden AB
Triethylamine	121-44-8	Fisher Scientific
Trypsin (for cell culture) (0.25 % Trypsin, 1x EDTA, Phenol Red)	-	Thermo Fisher Scientific (Gibco)
Tween 20	9005-64-5	Fisher bioreagents

Solutions: the PBS (1x) buffer (pH 7,4, with calcium and magnesium ions) pH was adjusted with a 1 M citric acid solution to pH 6,5 and 6. The buffers were used for the dynamic light scattering (DLS) measurement of NPs and later preserved in the fridge (4 °C) for future use. For a 5 M NaOH solution 20 g of sodium hydroxide was dissolved in 100 ml of dH2O. The solution was stored in the refrigerator at 4 °C.

2.1.1. Fluorescent probes

Two probes were used as model drugs for the loading of NPs: fluorescein diacetate (FDA) and 2′,7′-dichlorofluorescein diacetate (DC-FDA). FDA is a well-known viability probe that can cross biological membranes and be hydrolysed by esterases inside living cells, as demonstrated by Rotman and Papermaster [81]. Diacylfluoresceins, which are fluorescein-containing molecules, are frequently employed as substrates for esterase and lipase activity and for the delivery of molecules to cells. Moreover, fluoresceins can be reduced to form leuco-fluorescein (i.e., fluorescin) derivatives, which act as useful probes for ROS [82].

DC-FDA is a hydrophilic dye which remains in the cytosol and can be oxidized to produce 2′,7′-dichlorofluorescein which emits a strong fluorescent signal at excitation (λex) 490 nm and emission (λem) 523 nm. DC-FDA is a versatile probe that can react with a wide range of oxidants, with different reaction rates, making it an excellent tool to monitor oxidative stress and redox changes [83].

2.1.2. Lipopolysaccharide

LPS is one of the components of the outer membrane of Gram-negative bacteria. It is composed of lipid A (hydrophobic domain), O-antigen (hydrophilic distal oligosaccharide) and a core oligosaccharide. They are heat-stable endotoxins which in the membrane serve as a protection mechanism against bile salts and lipophilic antibiotics [84] and help the bacteria to interact with other surfaces. It has been found that the hydrophobic anchor lipid A is by far the most bioactive component causing the endotoxicity of LPS and the receptor complex CD14/TLR4/MD2 is responsible for stimulating the production of proinflammatory cytokines [85]. LPS have been used to research its structure, immunology, toxicity, biosynthesis and to promote the production of growth-promoting factors [86].

2.1.2. Ac-Dex and PBE-Dex polymer synthesis

Both of the polymers and NPs were synthesized by Dr. Gizem Erensoy and Endri Bardhi at Chalmers University of Technology. The acetalization of dextran was carried out following the procedure by Broaders et al [70]. In brief, dextran (1 g, 0,095 mmol) was weighed and dissolved in 10 ml of anhydrous dimethyl sulfoxide (DMSO) with constant nitrogen flooding and magnetic stirring. Once the solution was completely dissolved, pyridinium p-toluenesulphate (15,6 mg, 0,062 mmol) was added, followed by 2-methoxypropene (3,4 ml, 37 mmol) to initiate the reaction. The reaction was stopped with 0,5 ml of triethylamine (TEA). To achieve different ratios of cyclic to acyclic acetalization, the reaction was halted at different time points. For instance, a 35% cyclic acetalization was achieved by stopping the reaction after 10 minutes. The final polymer was precipitated with dH2O, centrifuged (4,600 g, RT, 20 minutes), and washed with distilled water (dH2O) (pH=8,5). The excessive amounts of TEA were removed by dialysis for two days against 5 litres of dH2O using Spectra/Por 3 Regenerated Cellulose 3,5 kDa MWCO tubing. After freeze-drying for two days using Labcono Freezedry 2,5 litres, version 10411E, at -58 °C and 0,010 mbar, the polymer was attained.

The synthesis method of PBE conjugated to dextran was derived from Manaster et al [72]. To attain PBE-Dex, PBE (1,1 g, 4,68 mmol) and N,N-Carbonyldiimidazole (CDI) (1,51 g, 9,36 mmol) were combined and dissolved in anhydrous dichloromethane. The resulting mixture was stirred at room temperature (RT) under nitrogen for one hour. To extract the resulting compound from the organic phase, the mixture was subjected to three washes with dH2O and one wash with a saturated sodium chloride solution, using a separation funnel. The dichloromethane was removed via rotary evaporation to obtain PBE-CDI. Next, the activated compound PBE-CDI (0,5 g, 1,54 mmol) was mixed with a solution of dextran (2,2 g, 0,22 mmol) and TEA (0,25 ml, 1,80 mmol) in N,N-dimethylformamide. The mixture was stirred overnight at RT under nitrogen. The resulting product was purified using dialysis and subsequently harvested through freeze-drying.

2.1.3. NP synthesis

Once the polymers were synthesized, they were dissolved in an organic solvent (acetone), DC-FDA was added to load the NPs and the mixture was loaded into a syringe. The aqueous phase consisted of a polyvinyl alcohol solution with different concentrations. The pH of the aqueous phase was adjusted using TEA and monitored with pH paper. The organic phase was then dripped into the aqueous phase either by hand or using a syringe pump. After successful mixing, the organic solvent was removed by applying a vacuum. Two purification methods were used: centrifugation and ultrasonication or dilution and tangential flow filtration. The dispersions were collected and cryoprotected with trehalose dihydrate. Finally, the dispersions were freeze-dried.

2.2. Method workflow

Figure 6 presents a summarized workflow of the study. In brief, two different fluorescent probes which represented a model therapeutic cargo were investigated to set up an ON/OFF model system under different biochemical conditions to test the stability and how the environment impacts the readout. A standard curve was made for both probes in order to later on calculate their concentration released from Ac-Dex 35% and Ac/PBE-Dex 35% NPs *in-vitro*. A cell-based model system was developed to set up the ON/OFF model in macrophages where the ON-state described the release of the fluorophore due to the decomposition of the NPs while the OFF-state was ideally characterized by no release of the model drug. For the first steps, detailed questions included 1) optimal concentrations of the probes and LPS needed to activate macrophages, 2) time to activation and 3) can this response be turned off though the addition of the anti-inflammatory drug prednisolone. After that, the NPs were characterized by measuring their size, PDI, drug loading and encapsulation efficiency. As the final step, the NPs loaded with the model fluorescent probes were investigated to detect their ON/OFF release in the macrophage system and to determine their cytotoxicity.

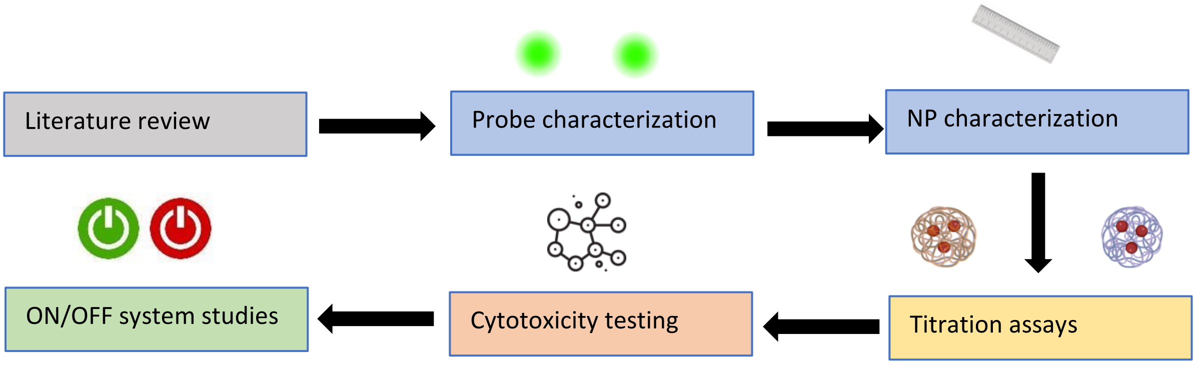

Figure 6. Outline of the thesis work process. The project included a literature review, characterization and optimization of the model fluorescent probes and NPs, cytotoxicity testing, and in-vitro testing of the ON/OFF/ON-system. Images adapted from Biorender.com (2023). [78]

2.2.1. Probe characterization

Two fluorescent probes, FDA and DC-FDA, were used as model drugs to determine their release from NPs and cell activation. For probe characterization, fluorescence standard curves were made in order to later on detect their concentration after release from NPs in the cytotoxicity assay. 5 mg of FDA was weighed in a 15 ml tube, dissolved in 4,9 ml of deionized water Milli-Q and 0,1 ml of 4 N NaOH was added to hydrolyze the dye and make it detectable in a microplate reader (Hidex Sense 425-301gi). A serial dilution was made between the range of 100-1000 ng/ml and 50, 100, 250, 500 and 600 ng/ml concentrations were used to plot the standard curve. The concentrations were plated in triplicates with one well left empty between the samples to avoid any cross contamination. The fluorescence was read at λex=490 nm and λem=520 nm. For DC-FDA, a similar protocol was used except 5 mg was dissolved in 1 ml of DMSO and λex=485 nm and λem=520 nm. All following assays including FDA or DC-FDA were measured at the same wavelengths as for the probe characterization.

2.2.2. Characterization of NPs

For the characterization of NPs, the size (hydrodynamic diameter) and PDI were measured with the DLS method (Zetasizer ZS, Malvern Panalytical) using disposable cuvettes (VWR, Polystyrene, 1,5 ml). First, 1 mg of the freeze-dried NPs were weighed and dissolved in 1 ml of dPBS. Next, they were centrifuged for 20 minutes at 4°C and 14 000 rpm to get rid of the cryoprotectant trehalose. The supernatant was removed and the NPs were resuspended in 1 ml of dPBS at pH 7,4, 6,5 and 6 to determine their stability and characteristics in different environments.

2.2.3. Model drug loading and encapsulation efficiency

The quantity of a drug present in a particle is known as drug loading, where a percentage value indicates the amount of the drug in a known mass of particles (Equation 1). Encapsulation efficiency, on the other hand, refers to the proportion of the drug used during formulation that can be recovered after the particles have been prepared (Equation 2). Since drug loading is limited, increasing the drug amount can lead to lower encapsulation efficiency. Encapsulation efficiency is useful for production purposes, while drug loading provides information on the number of particles needed to achieve a therapeutic response.

Equation 1. Model drug loading (%) calculation for NPs. A standard curve was used to determine the mass of DC-FDA, whereas the mass of the NPs was determined through weighing after freeze-drying.

$$model\ drug\ loading\ (\%) = \frac{m_{encapsulated\ model\ drug}\ (mg)}{m_{NP}\ (mg)} \cdot 100$$

Equation 2. Encapsulation efficiency (%) calculation of DC-FDA in the NPs. It was determined by dividing the total amount of the probe present in the NPs by the initial weighed amount of the probe. Alternatively, the model drug loading was used to quantify the total amount of drug incorporated within the NPs.

$$encapsulation\ efficiency\ (\%) = \frac{m_{encapsulated\ model\ drug}\ (mg)}{m_{model\ drug}\ (mg)} \cdot 100 = \frac{drug\ loading\ (\%) \cdot m_{NP}\ (mg)}{m_{model\ drug}\ (mg)}$$

2.3. Cell studies

2.3.1. Macrophage cell line

Raw264.7 murine macrophage cell line strain BALB/c was used in all of the assays. The cell line originates from a tumour in a male mouse induced with the Abelson murine leukaemia virus and is adherent.

2.3.2. General cell culturing

All cell procedures were carried out in Dulbecco's Modified Eagle Medium (DMEM) complete medium which contained 10% fetal bovine serum (FBS) to help cells grow, proliferate and attach, L-glutamine (GlutaMax) which provides amino acids for rapidly dividing cells, and DMEM. Media was always heated at 37 °C for 15-20 minutes in a bead bath to reach its normal pH of 7-7,6 and the optimal temperature for cells.

To thaw cells, first they were thawed by hand from -150 °C and then taken under a hood. 1 ml of DMEM complete medium was added drop by drop to the tube which contained DMSO, a cryoprotective agent. The cell suspension was transported to a 15 ml tube and 11-13 ml of complete medium was added. The tube was centrifuged at 0,2 x g for 5 minutes and if a pellet had not formed by then, the time and speed were increased. The supernatant was discarded and the pellet was resuspended in 1 ml of fresh medium. The cell suspension was transferred to a T75 cell culture flask along with 9 ml of pre-warmed DMEM complete medium and incubated at 37 °C and 5% CO_2 for several days.

Cell splitting was carried out when cells had reached 90% confluency which was determined by monitoring the culture with a light microscope. If cell density looked too low, only the medium was replaced every two days. The precise steps for cell splitting can be found in Appendix 1 Cell splitting protocol.

Seeding a surface treated 96-well tissue culture plate was carried out during the cell splitting. A density of 50 000 cells per well was used in assays. To determine the needed cell volume for plating, Equation 3 was used. The cell suspension was prepared on a reservoir and 100 µl was transferred to each well using a multichannel pipette. 100 µl of dPBS was pipetted in the outer rows of the plate to avoid evaporation from samples.

Equation 3. Calculation for cell volume needed in seeding a 96-well plate.

$$cell\ volume = \frac{0{,}5\ \cdot 10^6\ (cell\ concentration/ml) \cdot 10\ (ml)}{mean\ cell\ concentration/ml}$$

2.3.3. FDA and DC-FDA titration and time-dependency assays

To determine the optimal concentration of FDA for use in later assays, three different assays were carried out with Raw264.7 murine macrophage cell line. A 96-well plate was seeded 24 hours earlier with 100 ul of 50 000 cells per well (see 2.3.2. General cell culturing). The next day 100 µl of 10, 1, 0,1 and 0,01 µg/ml concentrations of LPS were added to activate the cells. In addition, 20, 10, 5 and 1 µg/ml concentrations of FDA were prepared by dissolving a 25 mg/ml stock in dPBS and performing a serial dilution. 20 µl of every concentration was added to corresponding rows. The assays included negative controls with cells and different FDA concentrations but no LPS and media controls with FDA but no added cells or LPS. After three hours of incubation, the plate was transferred to a plate reader which measured the FI every ten minutes for one hour. The assay was repeated thrice. Two titration and time-dependency assays were carried out for DC-FDA in a similar way.

2.3.4. LPS titration and time-dependency assays

LPS concentrations 1 and 0,1 µg/ml were tested on macrophages to determine whether there would be a difference in cell activation. A 96-well plate was seeded the day before the experiment (see 2.3.2. General cell culturing). The LPS dilutions were prepared from a 1 mg/ml stock in DMEM complete medium and 100 µl of the concentrations were added at one or three hours before the FI measurement to determine if there would be a time-dependent reaction. After the incubation at 37 °C and 5% CO_2, 20 µl of 5 µg/ml FDA was added to each well to detect the level of cell activation. The more activated the cells were, the more they would convert the fluorescent dye which would result in a higher FI. Inactivated cells and DMEM complete medium were used as controls. Along with FDA, two concentrations of prednisolone, 100 and 500 ng/ml, were added to induce an OFF-state in the activated cells. The FI was measured for one hour and 50 minutes.

2.3.5. Method development: biological ON/OFF/ON-system

The principle of the ON/OFF/ON-system was to activate the cells with LPS to induce an ON-state, then expose the cells to two concentrations of NPs and observe the effects on cell activation. The system was then switched OFF by adding prednisolone and back ON again by adding a second dose of LPS to observe the recovery of cell activation. The system was monitored by measuring the plate in the Hidex Sense plate reader every ten minutes to detect any changes in the FI in response to the different treatments. Figure 7 depicts the method set-up. The ON/OFF/ON-system was carried out according to the following steps:

1) prior to the day of the experiment, a 96-well plate was seeded with a cell density of 50 000 cells per well
2) 22-26 hours later the cells were activated with 100 µl of 1 and 0,1 µg/ml LPS doses and incubated for two hours at 37 °C and 5% CO_2
3) the media was replaced with 200 µl of dPBS and 20 µl of NPs with 500 and 250 µg/ml concentrations were added in triplicates to the cells
4) the plate was measured in a plate reader for 20 minutes after which 20 µl of prednisolone was added to induce the OFF-state
5) meanwhile a second batch of macrophages at a density of 10^6 cells/ml was incubated for two hours with LPS 1 and 0,1 µg/ml in T25 flasks. A cell scraper was used for detaching
6) the second measurement lasted for 40 minutes and 20 µl of pre-stimulated cells were added for reactivation of particle release
7) the FI of the plate was measured for an additional 40 minutes.

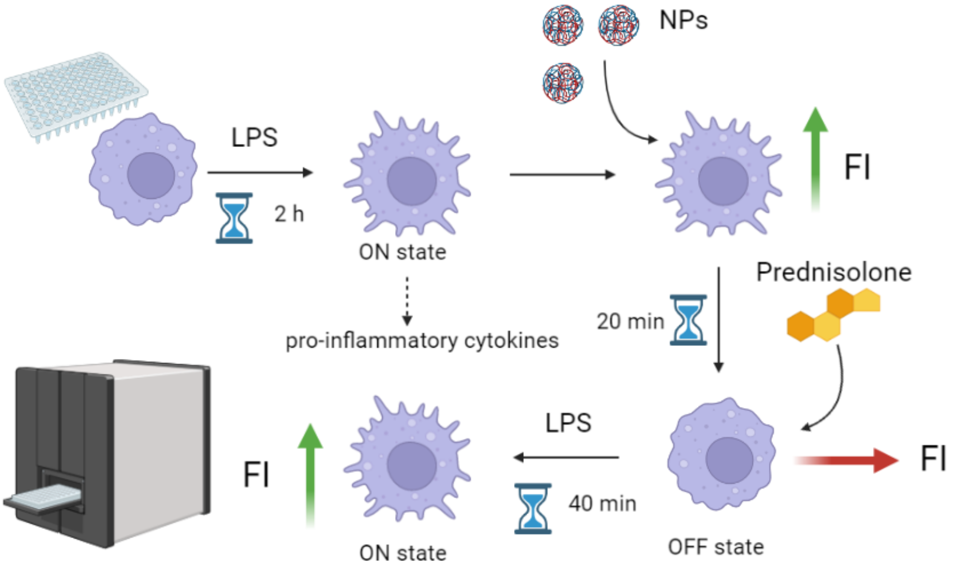

Figure 7. ON/OFF/ON-system study design. Image was created in BioRender.com (2023). [78]

2.3.5. Cytotoxicity assay

For the cytotoxicity assay, a 96-well plate was prepared the previous day by seeding 20 000 cells per well in 160 ul of DMEM complete medium containing a 1% penicillin and streptomycin mixture. The plate was incubated for 22-26 hours at 37 °C and 5% CO_2. To prepare the NPs stock, 2 mg was weighed in an Eppendorf tube, 1 ml of dPBS was added and the mixture was centrifuged for 25 minutes at 4 °C. The supernatant was removed and the pellet was dissolved in 2 ml of dPBS to get a final concentration of 1 mg/ml. The stock was vortexed for 1 minute and vigorously pipetted.

The following day 20 µl of a range of NPs and DC-FDA concentrations diluted in dPBS were added. Cells incubated with DMEM complete medium were used as a negative control and Triton X -100 1% as a positive control. The plate was incubated at 37 °C for 22-26 hours. 20 µl of 0,15 mg/ml resazurin reagent (Alfa Aesar) dissolved in sterile- filtered dPBS was added to all wells. The plate was incubated again for two hours and fluorescence was detected at λex=560 nm and λem=590 nm in a plate reader. The principle of this assay is based on the reduction of resazurin, a blue and non-fluorescent dye, to the red fluorescent dye resorufin by dehydrogenase enzymes. Living cells maintain a reducing environment within their cytoplasm and mitochondria. The amount of resorufin produced depends on cell viability: the more toxic a substance, the less dye is converted and the absorbance values are lower.

2.3.6. Enzyme linked immunosorbent assay

ELISA was carried out according to the manufacturers protocol [87]. First a high binding 96-well plate was coated with a rat monoclonal capture antibody that specifically targets mouse IL-6. 16-18 hours later after the antibody had attached to the bottom of the wells, the plate was washed four times with 200 µl of Wash Buffer. Residual buffer was blotted by firmly tapping the plate upside down on a tissue. The plate was washed and emptied in the same way between each step. To block non-specific binding and reduce background, 100 µl of Assay Diluent A was added to each well, the plate was covered with parafilm and incubated for one hour at RT on a plate shaker at 500 rpm. All subsequent incubations were carried out in the same conditions. Next 50 µl of the samples taken from LPS titration and time-dependency assays (see 2.3.4. LPS titration and time-dependency) and standards were added to the wells, allowing IL-6 to bind to the capture antibody and the plate was incubated for two hours.

Subsequently, a biotinylated rat monoclonal anti-mouse IL-6 detection antibody was introduced, which resulted in the formation of an antibody-antigen-antibody sandwich during a one-hour incubation. To complete the detection process, 50 µl of Avidin-HRP reagent was added and incubated for 30 minutes. For the last step, the plate was washed five times and the wells were soaked with Wash Buffer for one minute for each wash in order to reduce any background. This step was followed by adding 50 µl of the TMB substrate, which produced a blue colour proportional to the concentration of IL-6 in the wells. After 30 minutes of incubation in the dark, the reaction was terminated by adding Stop Solution, which caused the colour to change from blue to yellow. Finally, the absorbance of the wells was measured at 450 nm and 570 nm using a microplate reader immediately after adding Stop Solution.

2.4. Statistical analysis

The results are presented as the mean ± standard deviations for single assays and as standard errors for the means of multiple assays. The standard error was calculated by dividing the standard deviations with a positive square root count. The experiments were conducted in technical triplicates unless otherwise stated. To compare the differences between two groups, a two-sided t-test assuming unequal variances was used. For comparisons involving more than two groups, a single-factor ANOVA was conducted. For time-dependent analyses such as release studies, a two-way ANOVA analysis was performed. All calculations were carried out in Excel, and p-values less than 0,05 were considered significant.

3. Results and Discussion

3.1. Material characterization

3.1.1. Probe characterization

In order to quantify the amount of FDA and DC-FDA that was released from the particles, standard curves were made by measuring the concentration of the two probes in water at the wavelength of the corresponding excitation and emission. The values for FDA proved to be inconsistent and to get an acceptable R value, the standard curve was repeated several times (Figure 8). Initially there was no fluorescence detected because the dye needed to be hydrolysed. After adding NaOH, the dye became fluorescent and a signal was emitted. DC-FDA is known to be a more stable compound and its concentrations only needed to be measured once after hydrolysation (Figure 9).

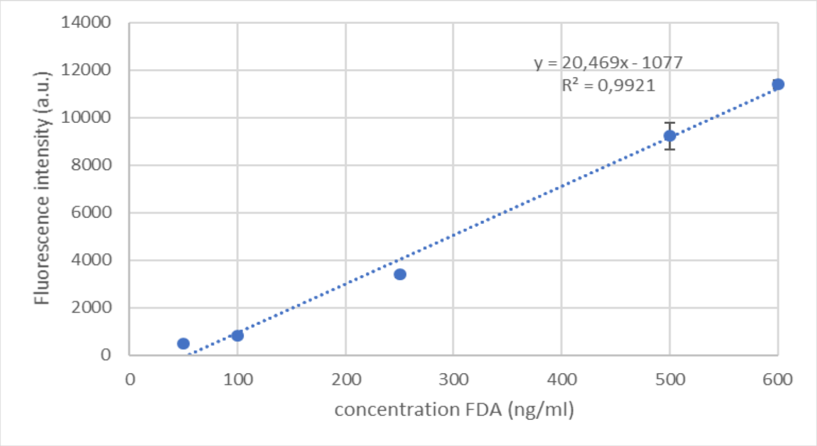

Figure 8. Standard curve of FDA in Milli-Q water. To demonstrate a concentration dependence, FDA was diluted to a concentration range of 0 to 600 ng/ml, and values were obtained at λex=490 nm and λem=520 nm to plot a standard curve. The experiment was carried out six times due to the instability of FDA (n=6).

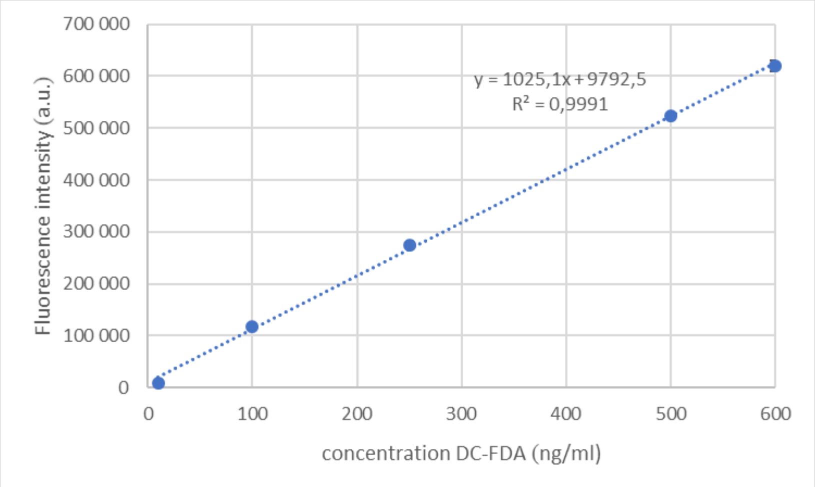

Figure 9. Standard curve of DC-FDA. DC- FDA was diluted to a concentration range of 0 to 600 ng/ml, and values were obtained at λex=485 nm and λem=520 nm to plot a standard curve. The experiment was carried out once (n=1).

3.1.2. Characterization of NPs

In order to effectively interact with the inflammatory area, drug-loaded NPs need to circulate in the bloodstream for an adequate duration. However, conventional NPs with non-modified surfaces often get trapped in the reticuloendothelial system, particularly in organs like the liver and spleen, depending on their size and surface properties [88]. Therefore, the characteristics of particles such as size and PDI play a crucial role in targeted drug delivery. The hydrodynamic sizes and PDI of Ac-Dex 35% NP and Ac/PBE-Dex 35% NP loaded with DC-FDA are shown on Figure 10 and Figure 11. Both the NPs and the supernatant were measured with DLS to confirm their presence and absence in the supernatant since no visible pellet was formed after centrifugation.

The particles loaded with FDA were excluded from the ON/OFF/ON studies due to their abnormal size and PDI. However, the standard curve of FDA and titration assays done with them are still presented (see 2.2.1. Probe characterization and 2.3.3. FDA and DC-FDA titration and time-dependency assays). After characterization with nuclear magnetic resonance spectroscopy (NMR), it became clear that Ac/PBE-Dex didn't contain any PBE and that it consisted only of stabilized Ac-Dex. In spite of that the NPs containing the so-called Ac/PBE-Dex were used in assays as a stable comparison to the other NPs and the polymer will be still referred to as Ac/PBE-Dex.

At pH 7,4, 6,5, and 6,0, the hydrodynamic sizes for Ac-Dex 35% NPs were 167 nm, 240 nm, and 256 nm, respectively, and for Ac/PBE-Dex 35% NPs were 237 nm, 422 nm, and 423 nm, respectively. To determine the statistical differences of the sizes at different conditions, a one-way ANOVA was conducted. The pH affected both types of the NPs ($p<0,05$): the lower the pH, the more the size increased. With Ac-Dex 35% NPs the average size increased 73 nm between pH 7,4 and 6,5 and 16 nm between pH 6,5 and 6. Ac/PBE-Dex 35% NP size increased 185 nm between pH 7,4 and 6,5 and 1 nm between pH 6,5 and 6. This could be attributed to swelling or aggregation [89]. Acidic conditions can lead to changes in the surface charge or hydration state of the NPs, causing them to interact differently and aggregate or swell, resulting in an overall increase in size.

Ac-Dex 35% NPs had a PDI of 0,29 at pH 7,4 which significantly decreased ($p=0,007$) to 0,25 at pH 6,5 and to 0,15 at pH 6 indicating a more uniform size distribution. Ac/PBE-Dex 35% NPs showed an opposite trend where the PDI increased from 0,16 at pH 7,4 and 6,5 to 0,22 at pH 6 but the change was not considerable ($p=0,41$). The size distribution of Ac/PBE-Dex 35% NPs remained relatively consistent across the tested pH values and prove that they could be used as a stable reference in assays.

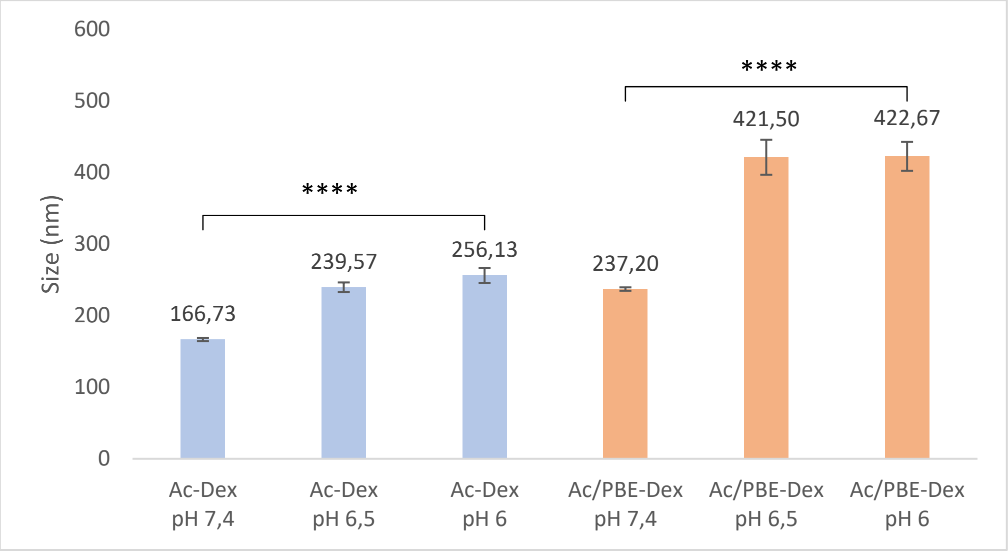

Figure 10. Size of Ac-Dex 35% NP (Ac-Dex, marked in blue) and Ac/PBE-Dex 35% NP (Ac/PBE-Dex, marked in orange) loaded with DC-FDA. Sizes were determined using pH-adjusted dPBS (pH 7,4, 6,5 and 6) for measurements after freeze-drying. Measurements of the loaded NPs were performed once (n=1) with three technical replicates. **** - p≤0,0001.

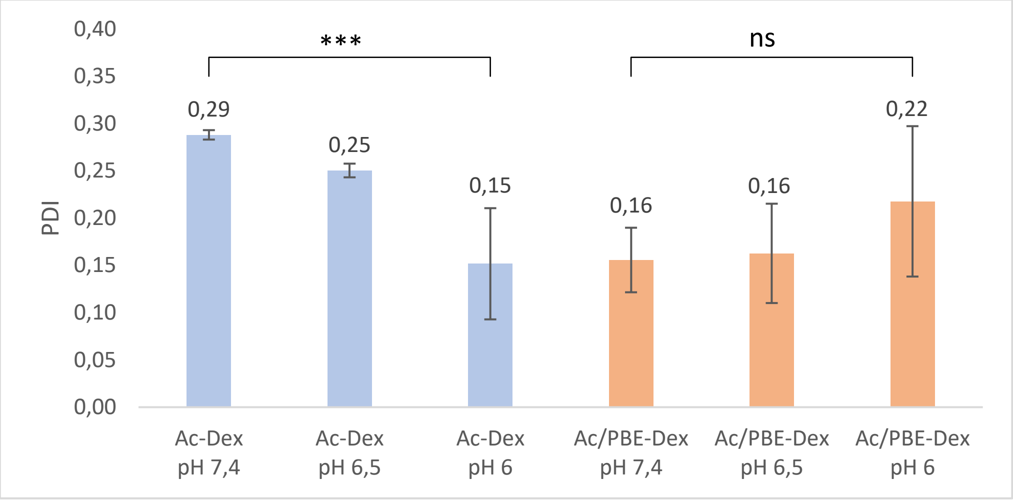

Figure 11. PDI of Ac-Dex 35% NP and Ac/PBE-Dex 35% NP loaded with DC-FDA. PDIs were determined using pH-adjusted dPBS (pH 7,4, 6,5 and 6) for measurements after freeze-drying. Measurements of the loaded NPs were performed once (n=1) with three technical replicates. *** - p≤0,001, ns - p>0,05.

3.1.3. Model drug loading and encapsulation efficiency

The anticipated model drug loading of 1% was not confirmed upon measuring the NPs (Figure 12). The mean loading for Ac-Dex 35% NPs was 0,119% and for Ac/PBE-Dex 35% NPs it was 0,082%. Ac-Dex 35% NPs achieved significantly higher loading (p<0,05). It suggests that the choice of polymer formulation, specifically the use of Ac-Dex 35%, was more effective in achieving the desired loading outcome. The encapsulation efficiencies for the NPs were 0,1073% and 0,0708% (Figure 13). It is important to note that the encapsulation efficiency values were derived from theoretical projections due to methodology issues; thus, they may not precisely reflect the empirical conditions.

The drug loading of NPs can exhibit significant variability, often influenced by the fabrication process [90]. There are several advantages to formulating NPs with higher drug loading: a higher drug loading reduces the need for non-active excipients, as the same quantity of active pharmaceutical ingredient can be achieved with fewer additional components in the NP formulation. Additionally, a higher drug loading enables the delivery of an equivalent dose of the active ingredient with a lower number of particles. This reduction in the number of NPs required for the desired dose can lead to benefits such as decreased manufacturing and processing time, reduced raw material consumption, and lower energy requirements. This is particularly relevant as many NP manufacturing processes involve the input of mechanical energy. The low encapsulation efficiency suggests that a significant amount of the substance was lost or not effectively incorporated into the NPs. This could lead to poor bioavailability of the drug [91]. Encapsulation of hydrophobic drugs can be improved by changing the solvents used for solubilization or the preparation method.

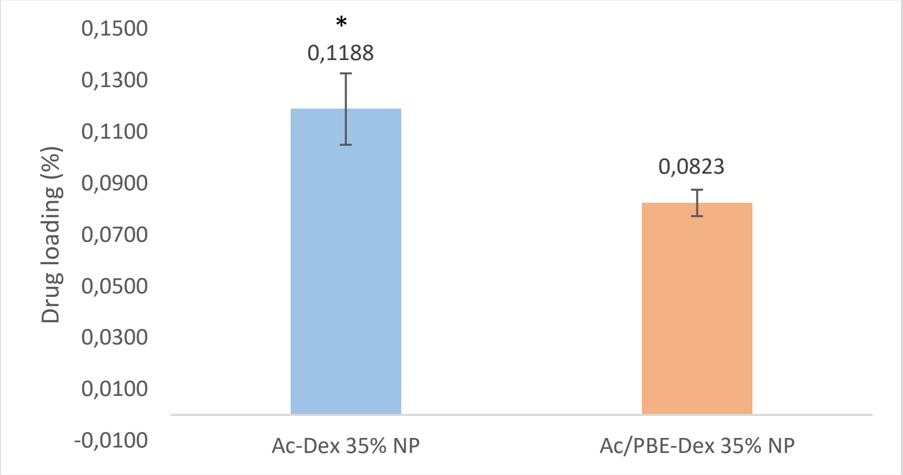

Figure 12. Model drug (DC-FDA) loading of Ac-Dex 35% NPs and Ac/PBE-Dex 35% NPs. The NPs were synthesized using nanoprecipitation. The mean of technical triplicates and the standard deviations are shown. * - p≤0,05.

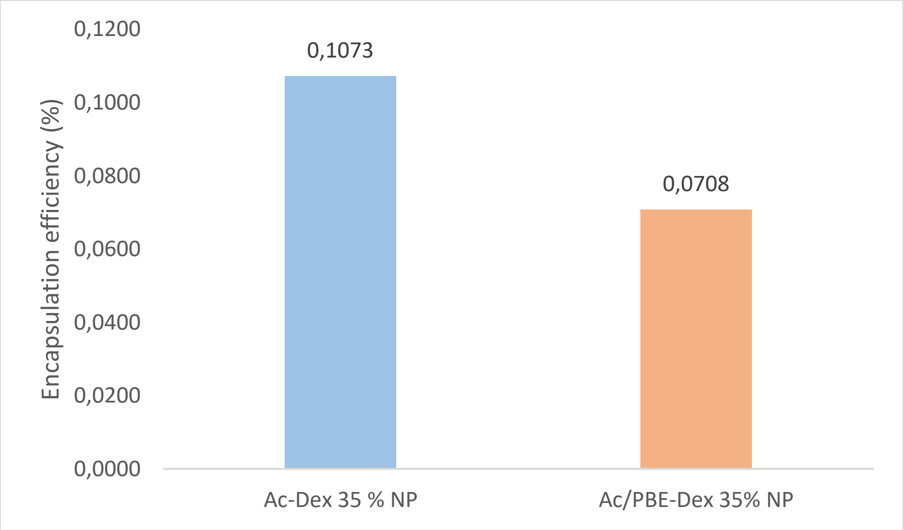

Figure 13. Encapsulation efficiency of Ac-Dex 35% NPs and Ac/PBE-Dex 35% NPs loaded with DC-FDA. Standard deviations are not represented in the data due to the nature of these values being derived from theoretical computations.

3.2. Cell studies

The purpose of the cell studies was to determine if the NPs were inflammation specific, more accurately would they degrade at a lower pH and release the model drug which could then be converted by cells into a fluorescent component. In brief, the investigation process was as follows: titration assays were carried out for both of the probes, LPS and prednisolone. Cell activation was confirmed with an ELISA and the biocompatibility of the NPs was tested with a cell viability assay. To induce an inflammatory state in Raw264.7 macrophages they were activated with two concentrations of LPS. Prednisolone was added to turn the cells off which should be reflected in a stabilized FI signal. To reactivate the cells, fresh cells incubated with LPS in the same condition as the first batch were added to the corresponding wells. Activated cells with no prednisolone and no second round of added cells were used as negative controls.

3.2.1. Pre-testing FDA and DC-FDA concentrations with different LPS doses

FDA concentration 20 µg/ml was left out after the first assay because it was determined to be too high and didn't correspond to data found in literature. The assays carried out with FDA produced inconclusive results between the four LPS concentrations and the observed variability, as indicated by large standard errors, was considerable (Figure 14-16). There is a significant increase in FI values from 1 to 10 µg/ml, exhibiting a dose-dependent response ($p<0,001$). Due to high FI values with the maximum concentration and poor detectability of the lowest concentration, FDA 5 µg/ml was chosen to use in the LPS titration and time-dependency assays (see 3.2.2. Optimizing LPS and prednisolone concentrations and time).

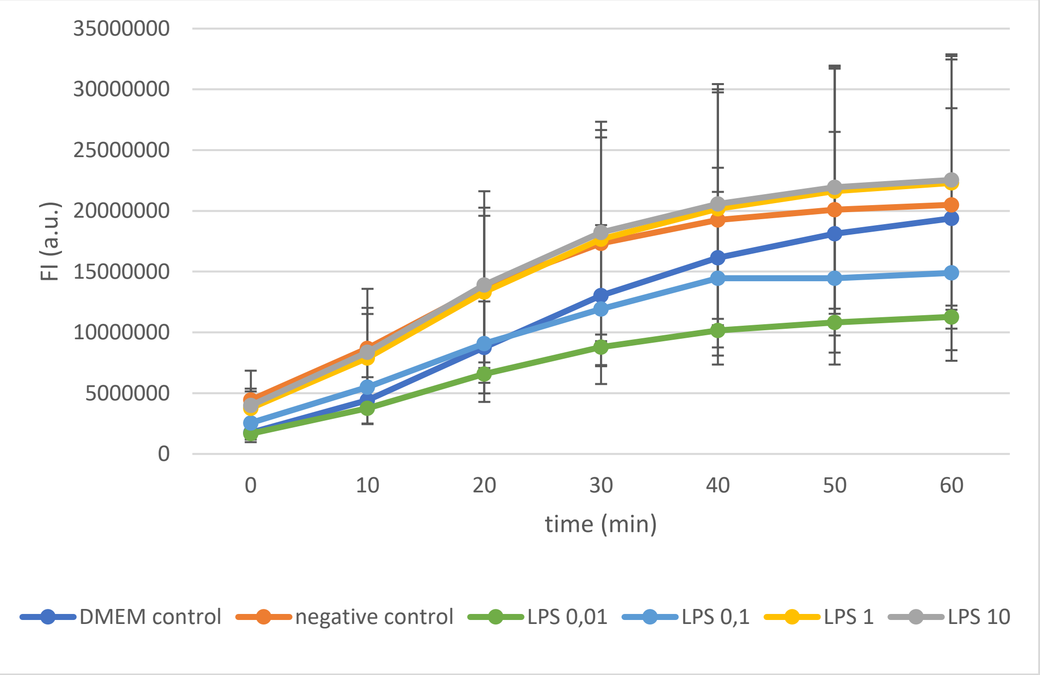

Figure 14. Fluorescence intensity of FDA 10 µg/ml tested on cells activated with LPS 0,01, 0,1, 1 and 10 µg/ml. Negative control represents non-activated cells and negative control with FDA 10 µg/ml corresponds to non-activated cells with added FDA. The means and standard errors of two assays (n=2) are shown.

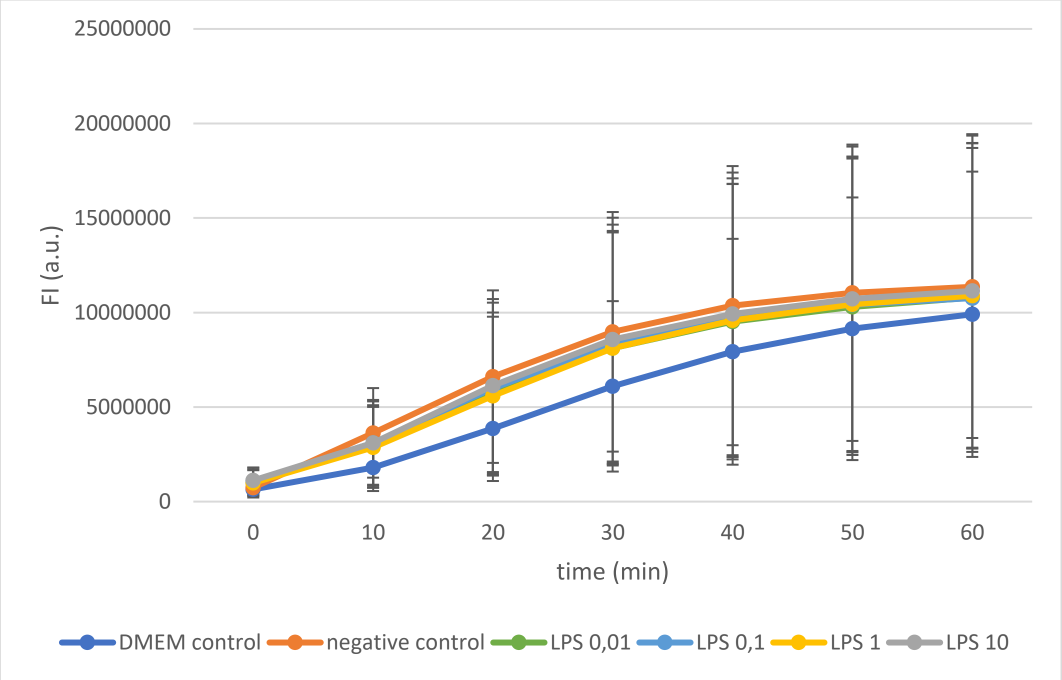

Figure 15. Fluorescence intensity of FDA 5 µg/ml tested on cells activated with LPS 0,01, 0,1, 1 and 10 µg/ml. Negative control represents non-activated cells and negative control with FDA 5 µg/ml corresponds to non-activated cells with added FDA. The means and standard errors of two assays (n=2) are shown.

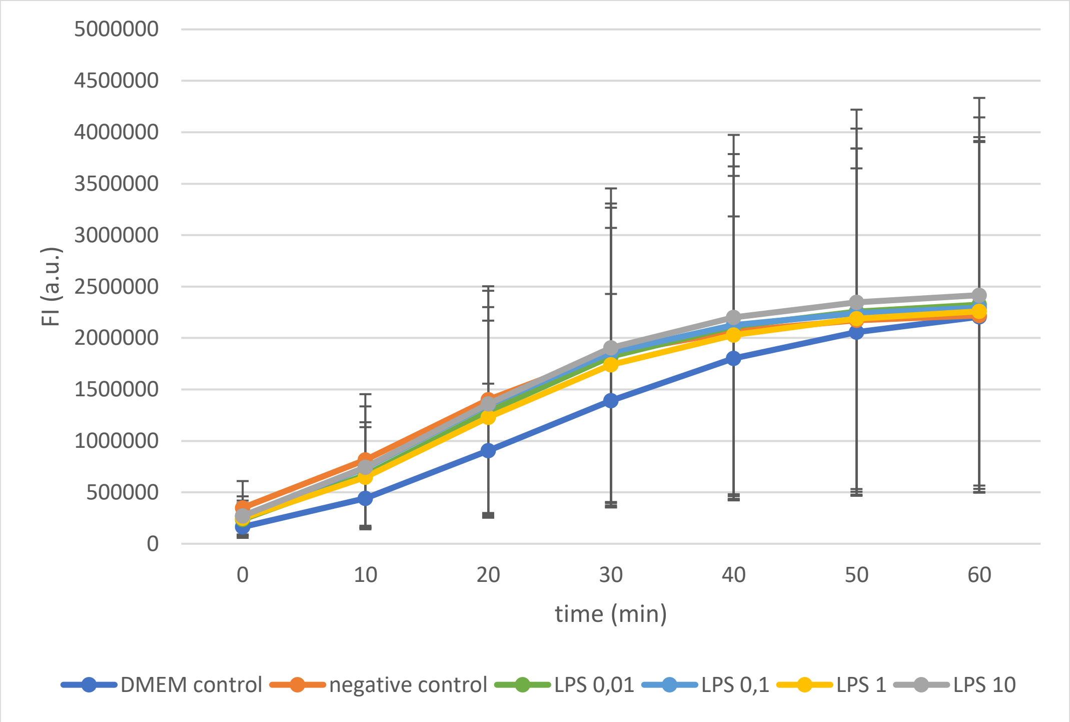

Figure 16. Fluorescence intensity of FDA 1 µg/ml tested on cells activated with LPS 0,01, 0,1, 1 and 10 µg/ml. Negative control represents non-activated cells and negative control with FDA 1 µg/ml corresponds to non-activated cells with added FDA. The means and standard errors of two assays (n=2) are shown.

The first three FDA and LPS titration assays did not yield any coherent results and the samples had different values every assay. The negative control's FI values were sometimes higher compared to

LPS activated cells which led to suspect that one of the DMEM complete medium components was hydrolysing FDA. It was confirmed that the DMEM complete medium itself converted FDA and even the media controls had almost as high fluorescence values as the activated cell samples. The hydrolysis of FDA in the absence of live cells is an issue that has been reported before and can lead to false interpretation of negative results [92]. To determine which medium component caused the hydrolysis, FDA was measured with each of the components separately (Figure 17).

The FIs of FBS, GlutaMax, and DMEM mixed with dPBS were measured to determine which one of them was causing FDA conversion. In addition, DMEM without phenol red was also measured as a possible substitute for the complete medium. The components with the highest FI values were dPBS+FBS, dPBS+GlutaMax+FBS, DMEM and DMEM complete medium. The differences with dPBS were significant (p<0,01). Since several of the media components proved to be hydrolysing FDA, it was decided to replace the cell medium with dPBS in future assays since that had the lowest signal. In the next assays before incubation in the plate reader, all complete media was aspirated from the wells and replaced with 200 µl of dPBS and 20 µl of 5 µg/ml FDA. The plate was placed in the plate reader for a one-hour measurement.

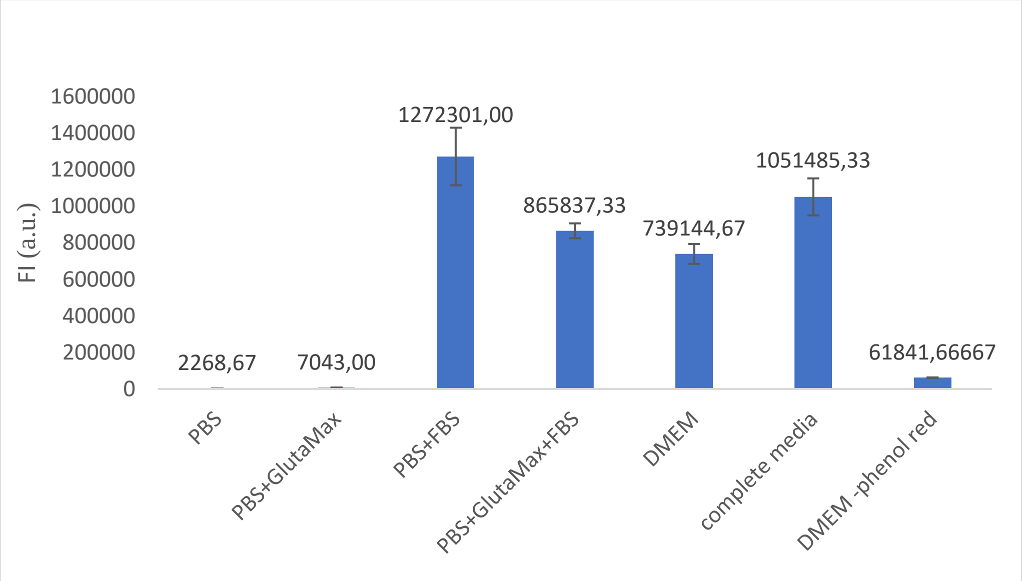

Figure 17. Fluorescence intensity of FDA at a concentration of 5 µg/ml. Each of the DMEM complete medium components was mixed with PBS and measured as triplicates. PBS – phosphate buffered saline, GlutaMax – L-glutamine, FBS – fetal bovine serum, DMEM – Dulbecco's Modified Eagle Medium, DMEM -phenol red – Dulbecco's Modified Eagle Medium without phenol red.

The titration assays with DC-FDA 10 µg/ml (Figure 18) and 5 µg/ml (Figure 19) showed that there were no significant differences between the LPS concentrations. With DC-FDA 1 µg/ml a slight deviation could be seen between LPS 10, 1 and 0,01 µg/ml and LPS 0,1 µg/ml where the 0,1 µg/ml concentration had a lower FI (Figure 20). However, statistical analysis showed that none of the LPS groups proved to have significant differences (p>0,05). A significant dose dependent response (p<0,01) can be seen as the FI values increase from 1 to 10 µg/ml.

One explanation for the similar responses to the different LPS concentrations is the saturation of cellular response: the cellular response to LPS reached a maximum or plateau, regardless of the LPS dose used. Once the cells were activated, they could only exhibit a maximal level of FI, and increasing the LPS dose further did not elicit any additional response. Other potential explanation could be the limitation in the binding capacity of LPS. If all available binding sites are occupied at lower concentrations of LPS, then increasing the LPS concentration would not further enhance the fluorescent intensity (FI) because there are no free binding sites for the additional LPS molecules. Additionally, the process of intracellular signalling may have self-limiting mechanisms that prevent excessive response. Once a certain level of activation is reached, these mechanisms may kick in, limiting further response even with increased LPS concentration [93]. This could be an evolutionary protective mechanism to prevent cell damage from an overly robust response. Finally, it's also possible that there might be a negative feedback mechanism in place that gets triggered when the response reaches a certain threshold, thereby keeping the response under check [94].

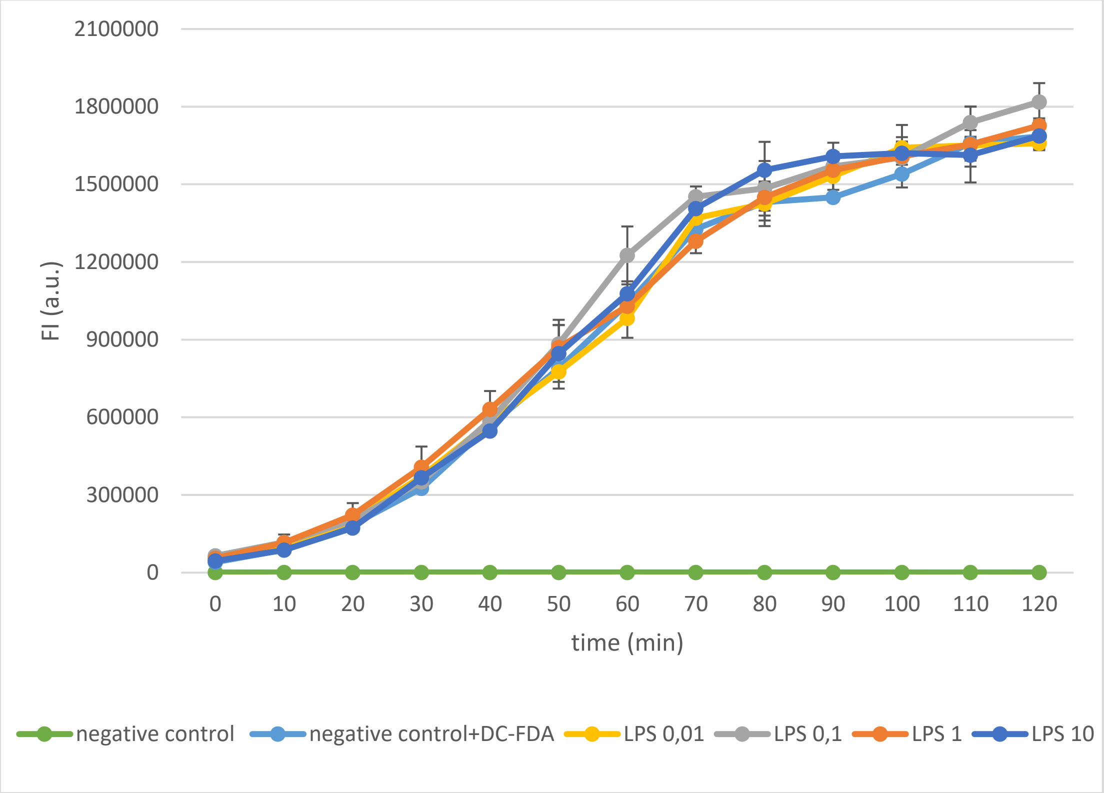

Figure 18. Fluorescence intensity of DC-FDA 10 µg/ml tested on cells activated with LPS 0,01, 0,1, 1 and 10 µg/ml. Negative control represents non-activated cells and negative control with DC-FDA 10 µg/ml corresponds to non-activated cells with added DC-FDA. The means and standard errors of two assays (n=2) are shown.

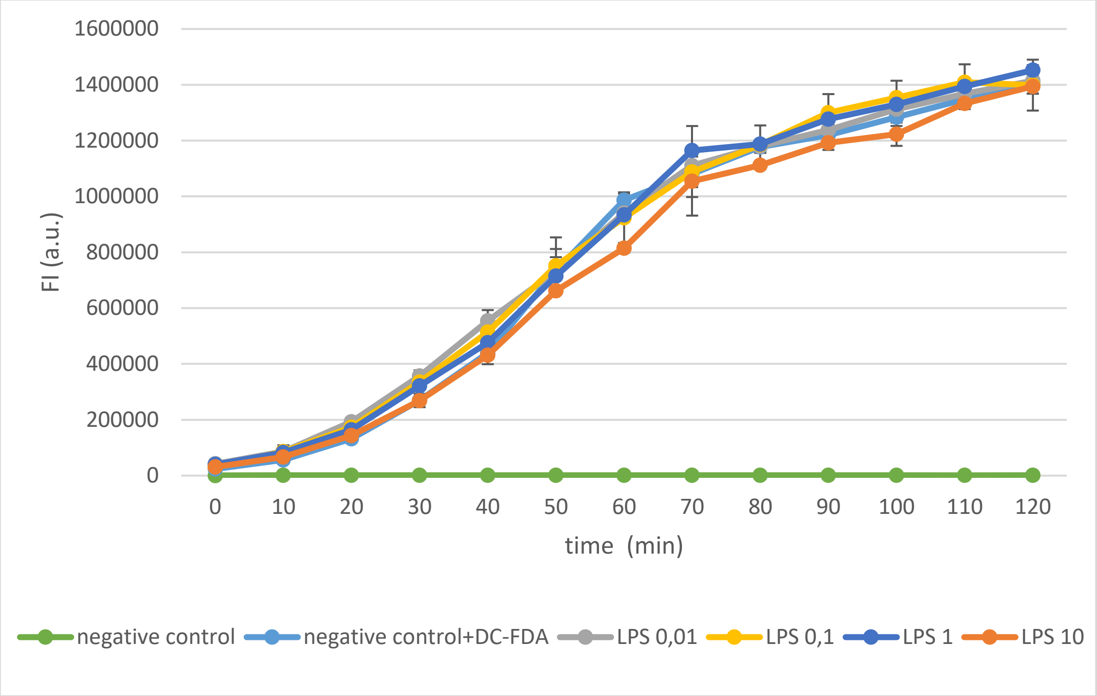

Figure 19. Fluorescence intensity of DC-FDA 5 µg/ml tested on cells activated with LPS 0,01, 0,1, 1 and 10 µg/ml. Negative control represents non-activated cells and negative control with DC-FDA 5 µg/ml corresponds to non-activated cells with added DC-FDA. The means and standard errors of two assays (n=2) are shown.

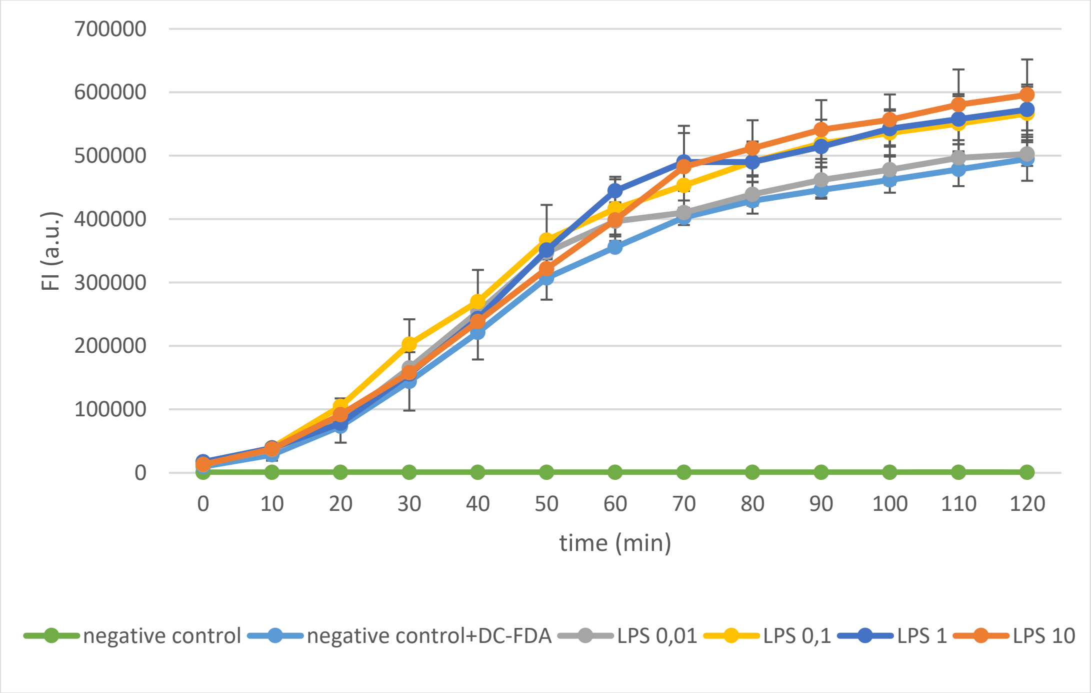

Figure 20. Fluorescence intensity of DC-FDA 1 µg/ml tested on cells activated with LPS 0,01, 0,1, 1 and 10 µg/ml. Negative control represents non-activated cells and negative control with DC-FDA 1 µg/ml corresponds to non-activated cells with added DC-FDA. The means and standard errors of two assays (n=2) are shown.

3.2.2. Optimizing LPS and prednisolone concentrations and time of incubation

Two concentrations of prednisolone, 180 and 500 ng/ml, were tested on cells stimulated with LPS 1 and 0,1 µg/ml for three and one hours (Figure 21-24). The first concentration of prednisolone was chosen based on previous cell studies and literature [95]. A higher concentration was added to see whether it had a more significant effect. Unstimulated cells with FDA were used as a negative control. Due to the different growth rates of macrophages, the standard errors are quite large. Nevertheless, the trends were similar in all the assays with prednisolone samples always having a lower signal.

There were significant differences between LPS 1 and 0,1 µg/ml stimulated cells and stimulated cells where prednisolone had been added. The FI of 180 and 500 ng/ml prednisolone samples was roughly two to three times lower at the end of the experiments. The differences in signal intensities began to appear already at 20-30 minutes which indicates the effectiveness of the drug. The FI for LPS 0,1 µg/ml was slightly lower but other than that the deviations between the stimulated cells and cells with prednisolone were similar. Unexpectedly the negative control also had a high FI even though those cells were unstimulated. No significant variations were observed between the two timepoints for LPS 1 and 0,1 µg/ml concentrations ($p=0,7$ and $p=0,8$, respectively) and because of that, two hours was chosen as the average for the incubation time with LPS.

Prednisolone is a synthetic glucocorticoid which reduces inflammation and has immunomodulating properties. It enters the cell nucleus and activates specific nuclear receptors by binding to them resulting in changed patterns of gene expression and lower levels of proinflammatory cytokines. In addition, prednisolone decreases the number of circulating lymphocytes, induces cell differentiation, and stimulates apoptosis in sensitive tumour cells populations [96]. Since the two concentrations tested proved to be both effective in reducing the FI, 500 ng/ml was chosen to continue with the ON/OFF/ON assays. These results suggest that prednisolone has the ability to attenuate the cellular response induced by LPS, regardless of the concentration used. Prednisolone likely interfered with the activation of cellular pathways and modulating gene expression involved in inflammation, leading to a dampened response to LPS stimulation and a reduced FI.

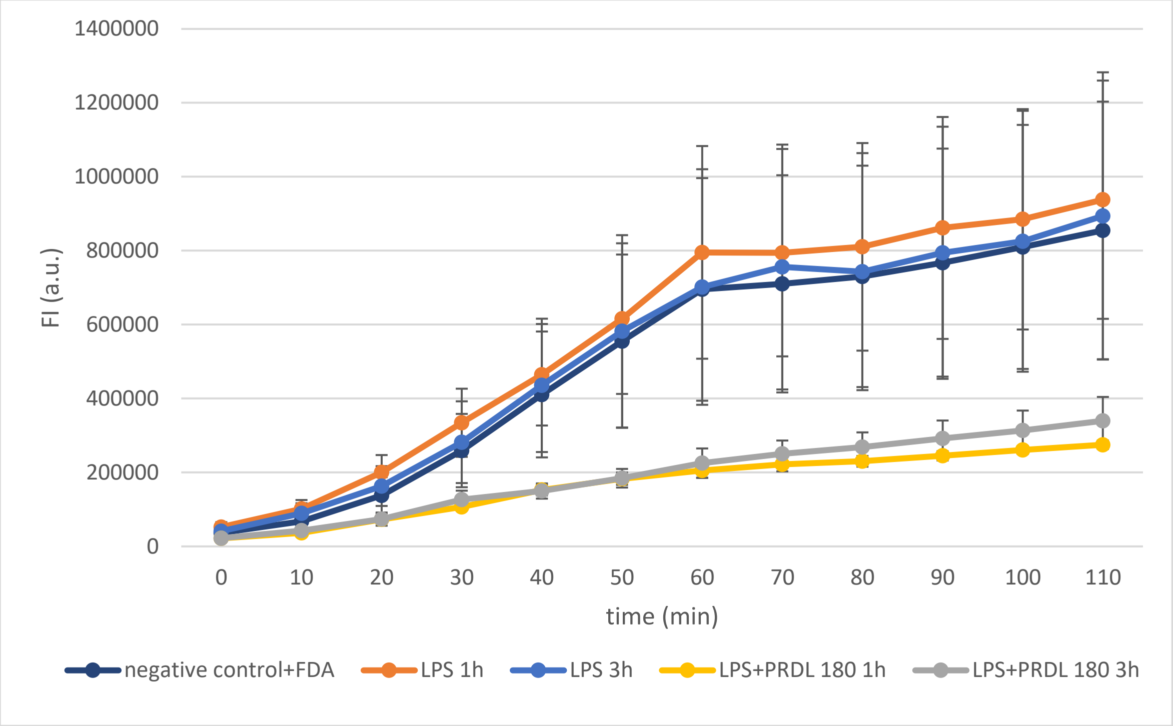

Figure 21. Fluorescence intensity of LPS 1 µg/ml activated cells and prednisolone 180 ng/ml samples. 5 µg/ml of FDA was added to each sample to monitor cell activation. FDA – fluorescein diacetate, LPS – lipopolysaccharide, PRDL – prednisolone.

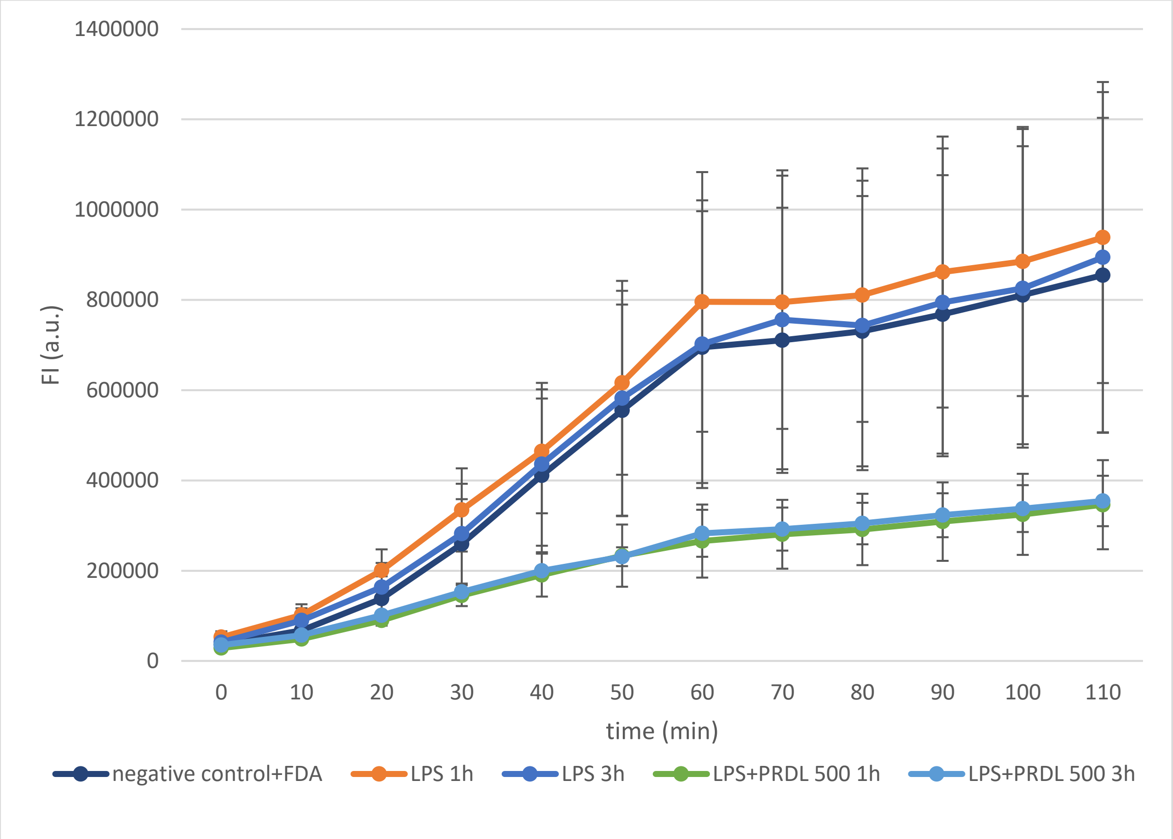

Figure 22. Fluorescence intensity of LPS 1 µg/ml activated cells and prednisolone 500 ng/ml samples. 5 µg/ml of fluorescein diacetate was added to each sample to monitor cell activation. FDA – fluorescein diacetate, LPS – lipopolysaccharide, PRDL – prednisolone.

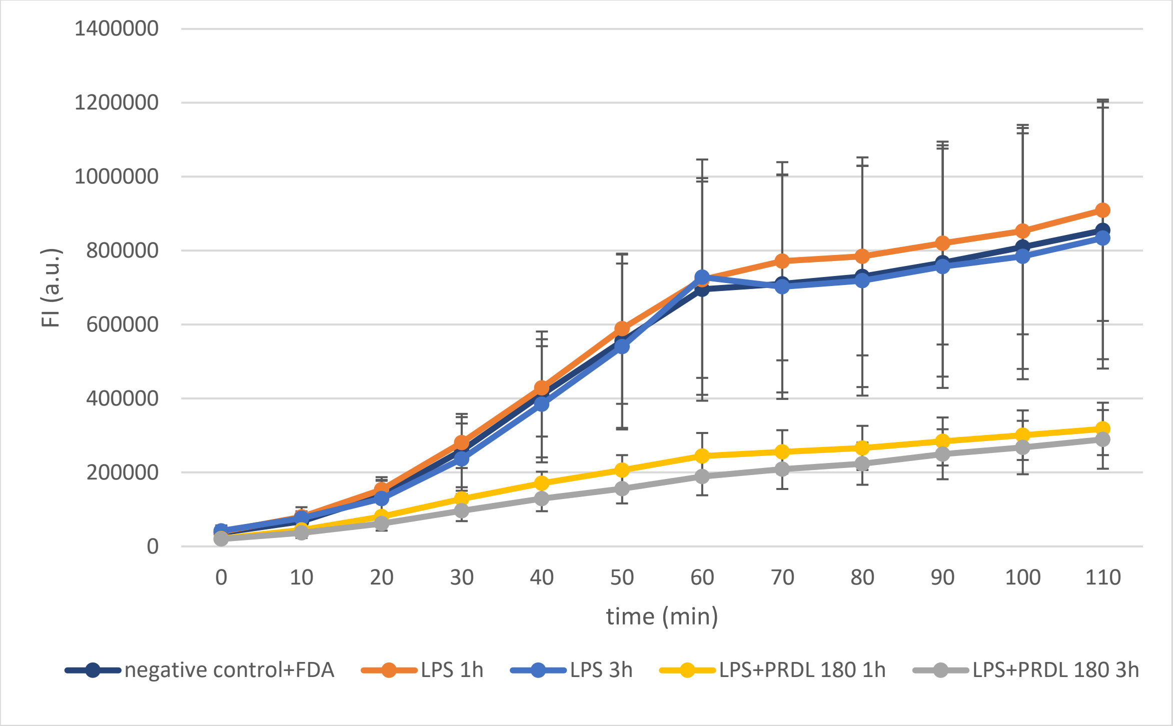

Figure 23. Fluorescence intensity of LPS 0,1 µg/ml activated cells and prednisolone 180 ng/ml samples. 5 µg/ml of FDA was added to each sample to monitor cell activation. FDA – fluorescein diacetate, LPS – lipopolysaccharide, PRDL – prednisolone.

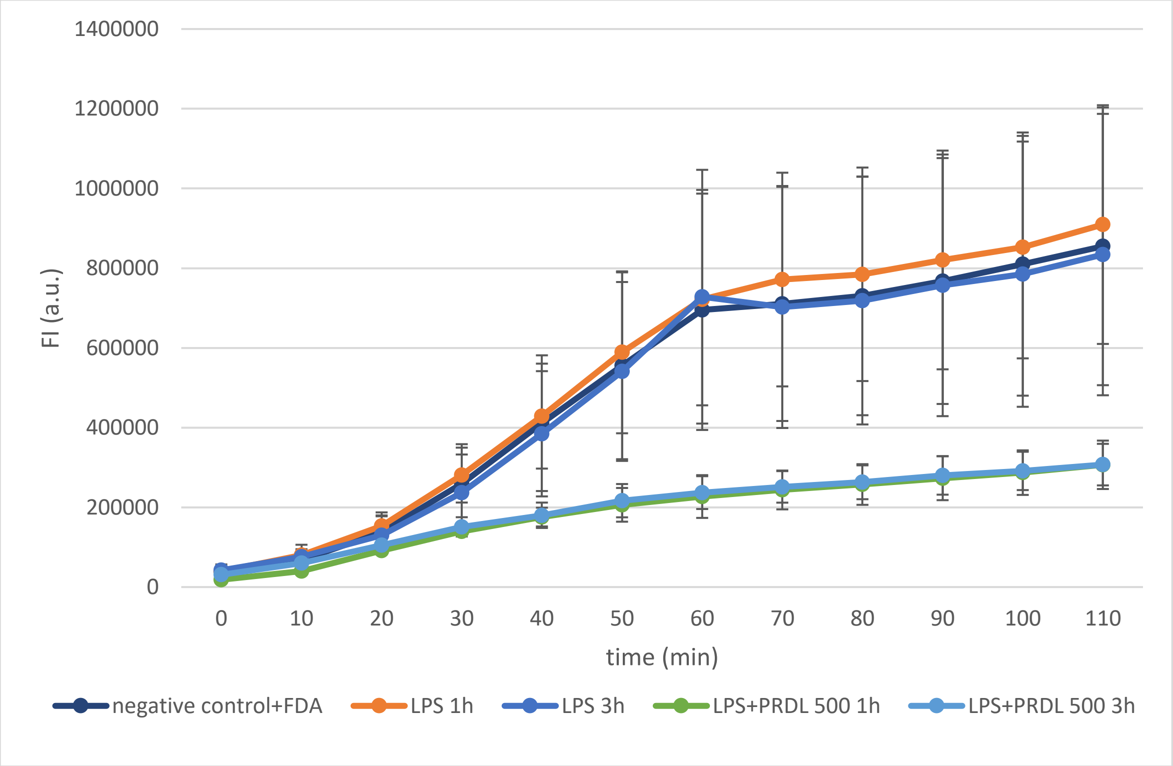

Figure 24. Fluorescence intensity of LPS 0,1 µg/ml activated cells and prednisolone 500 ng/ml samples. 5 µg/ml of fluorescein diacetate was added to each sample to monitor cell activation. FDA – fluorescein diacetate, LPS – lipopolysaccharide, PRDL – prednisolone.

3.2.3. ELISA

The gold standard of immunoassays is the ELISA, a labelled immunoassay. It is a highly sensitive immunological test that detects and measures a variety of substances, such as antibodies, antigens, proteins, glycoproteins, and hormones. In this thesis it was used to detect the production of IL-6 in order to confirm the activation of macrophages by LPS.

The level of IL-6 released in LPS stimulated controls and prednisolone samples was measured several times. At first, samples were diluted to 1:30 with cell medium, then 1:20, 1:10 until finally undiluted samples were used for the ELISA assay since some of the diluted samples did not give any readout. The assay with undiluted samples was performed twice (Figure 25). Due to the samples being thawed three times, the first assay produced higher levels of IL-6 than the second one which is why the standard deviations are larger. However, both of the experiments showed a similar trend where LPS samples which had been incubated for three hours had higher levels of IL-6 compared to samples incubated with LPS for one hour. Prednisolone proved to have no reducing effect on the production of IL-6 but this could be put down to a short incubation time: cells had been previously stimulated with LPS for three and one hours whereas the incubation time with prednisolone was one and a half hours. This seemed to not be a long enough period for the cells to turn off IL-6 production. Even though the effect of prednisolone couldn't be demonstrated with an ELISA, it could still be observed in assays where the FI was measured.

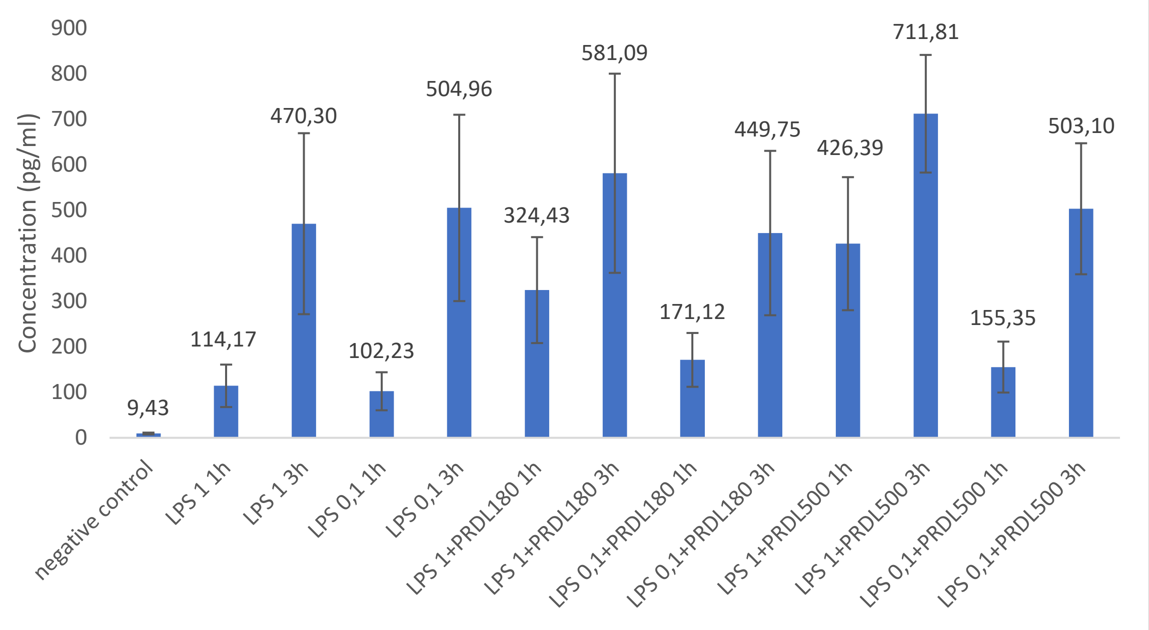

Figure 25. Release of IL-6 by LPS stimulated Raw264.7 macrophages depending on time (three and one hours) and concentration (1 and 0,1 µg/ml). Negative control represents unstimulated cells. LPS – lipopolysaccharide, PRDL – prednisolone. The means and standard errors of two assays (n=2) are shown.

Samples incubated with LPS for three hours had significantly higher levels of IL-6 compared to samples incubated for one hour ($p<0,05$). The observed difference in IL-6 levels suggests a time-dependent effect where the time of incubation with LPS used in the experiment influences the production and release of IL-6. A longer period of incubation appeared to elicit a more pronounced response in terms of IL-6 production compared to a shorter time. In addition, there was no significant difference observed between the corresponding timepoints of samples with LPS 1 µg/ml and samples with LPS 0,1 µg/ml.

3.2.4. Cytotoxicity assay

To ensure the safety and suitability of the NPs as a potential DDS for RA treatment, a thorough investigation of their biocompatibility was conducted using the resazurin-based cell viability assay according to the International Organization for Standardization (ISO) [109]. The primary objective was to assess whether the NPs, the cargo they carried, or degradation products posed any toxicity to cells. The principle of the resazurin viability assay relies on the mitochondrial respiratory chain in live cells, which reduces the oxidized non-fluorescent blue resazurin to the red fluorescent dye resorufin. The concentration of free DC-FDA was determined based on the encapsulated DC-FDA content within the NPs, calculated using the model drug loading and NP mass. According to ISO standards, cell viability below 70% is considered cytotoxic and therefore, the observed viability was compared to this threshold value.

Macrophages were treated with NPs in a range of 31,3-500 µg/ml and with the equivalent of free DC-FDA concentrations of 0,4625-7,4 µg/ml (Figure 26). After 24 hours NP concentrations 125 µg/ml showed a decreased viability, all the other samples were above or at the 70% viability level. To confirm whether there were relevant differences between the samples and the negative control with DMEM complete medium, a one-way ANOVA was conducted. It was found that no samples except for the positive control with Triton X-100 1% were statistically different from the negative control (p>0,05). Based on these findings, it can be concluded that the NPs demonstrated good biocompatibility.

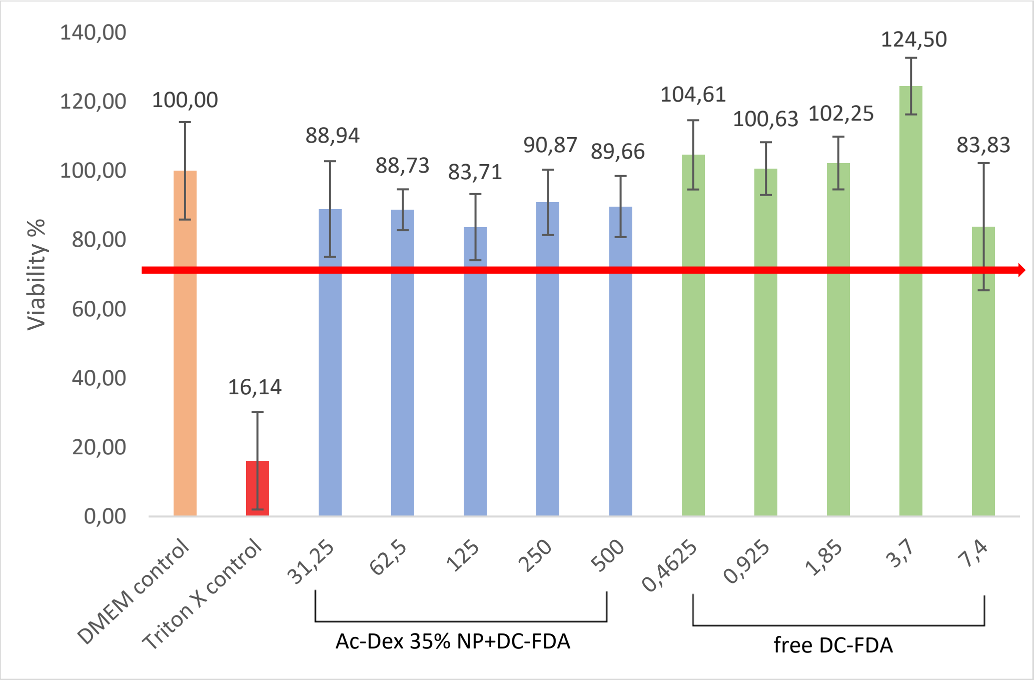

Figure 26. Viability of Raw264.7 macrophages after 24 hours exposure to NPs (blue) and DC-FDA (green). The resazurin assay was employed to evaluate the cytotoxicity of Ac-Dex 35% NPs loaded

with DC-FDA, as well as free DC-FDA. The experiment was conducted thrice (n=3), with three technical replicates for each control and concentration. The 70% cytotoxicity threshold is indicated by the red line.

3.2.5. ON/OFF-system

The objective of the designed DDS was to achieve pH-dependent release. To test this system, Raw 264.7 cells were stimulated with LPS to induce inflammation, the complete media was replaced with PBS and DC-FDA loaded Ac-Dex and Ac/PBE-Dex 35% NPs were added. The concentrations of NPs were selected based on previous titration assays. The FI was monitored for 20 minutes before prednisolone was added. The plate was measured again for 40 minutes and a new dose of LPS cells was added to get an ON state again. Raw 264.7 cells stimulated with LPS and no prednisolone added served as the control.

Figure 27 illustrates the ON/OFF FI of DC-FDA treated with Ac-Dex NPs and prednisolone for two hours and 50 minutes. Even though there is a crossover between the prednisolone sample and control, it was not a statistically significant difference (p>0,05). Figure 28 depicts the same system for Ac/PBE-Dex NPs where the controls and samples followed the same pattern. This trend suggests that prednisolone stimulated cells incorporated the same amount of DC-FDA compared to the controls. It was hypothesized that the dose of prednisolone was not high enough. To test this hypothesis, the concentration was raised from 500 ng/ml to 1000 and 5000 ng/ml. However, this also did not have a visible effect on cell activity. In the next assays a fresh prednisolone stock was prepared to exclude the possibility that freeze-thawing affected the chemical properties of previously prepared stock. Preparing a new stock did not improve the effect of the glucocorticoid.

Therefore, it was concluded that the proposed *in vitro* model, using DC-FDA to monitor drug release from Ac-Dex 35% NPs and Ac/PBE-Dex 35% NPs, proved to be a challenging system due to complications in the biological system in. The cells could not be deactivated repeatedly meaning that the model was not yet reproducible. Another option to enhance the specificity of the DDS is to use targeted drug delivery. This method involves NPs to which the drug is attached via ligands or antibodies functionalized on the surface to increase the NPs' targeting to specific antigenic proteins or cell membrane receptors [97]. Scientists use small ligands such as folate, class A scavenger receptors, and galactose to modify nanodrugs to target different receptors overexpressed on the macrophages' exterior [98]. Targeted drug delivery could also lead to personalized medicine, where treatments are designed specifically based on the individual's cellular profile.

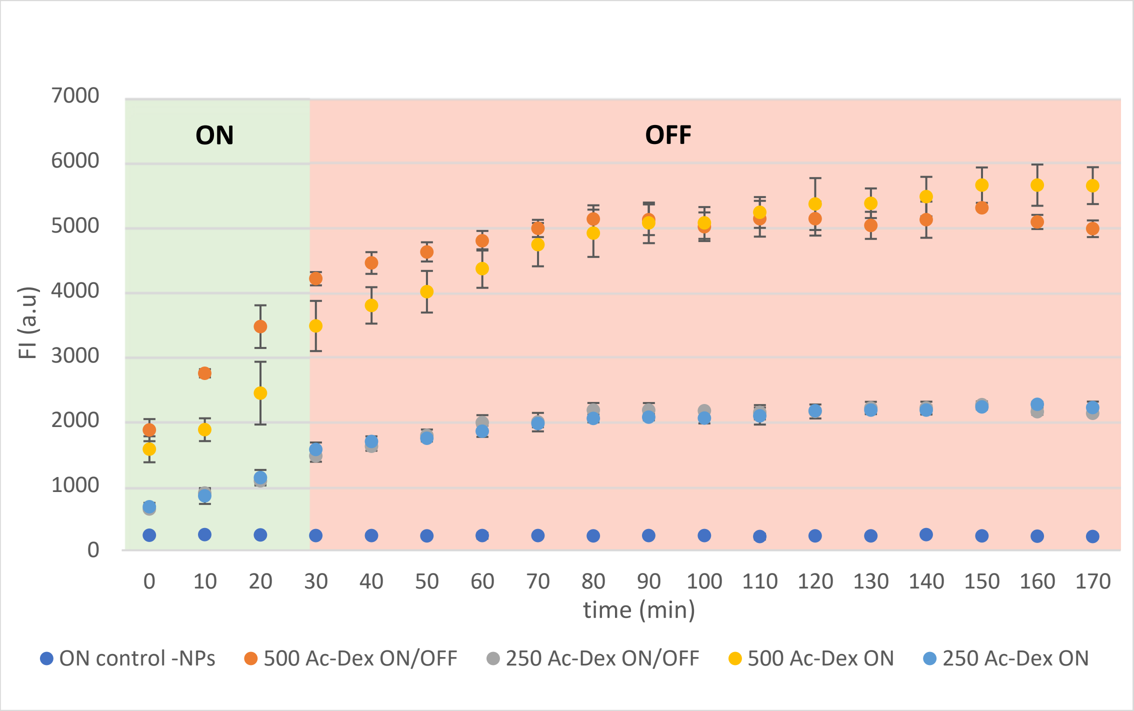

Figure 27. ON/OFF system of DC-FDA release from Ac-Dex 35% NPs. The NPs were centrifuged and resuspended in dPBS before use. Cells were pre-stimulated with LPS 1 µg/ml for two hours to get the ON-state (marked green). After the addition of the particles, the release of DC-FDA was measured. To induce the OFF-system, prednisolone was added to shift the pH from slightly acidic to pH 7.4 and the measurement was continued (marked red). Experiments have been conducted once (n=1) with three technical replicates.

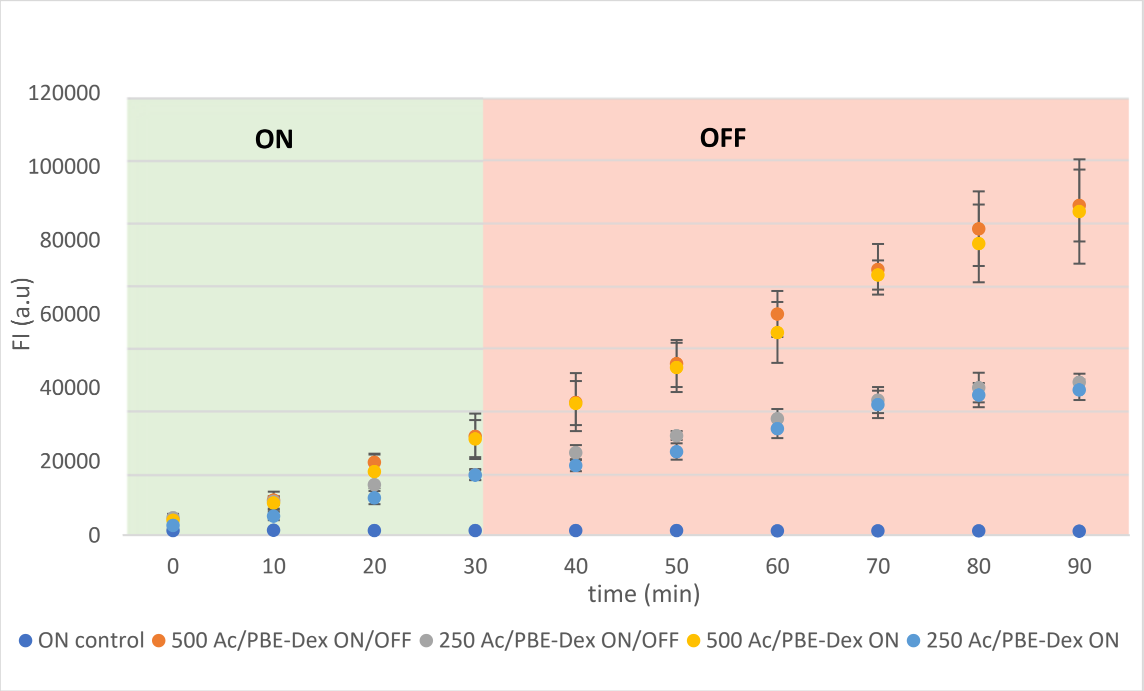

Figure 28. ON/OFF system of DC-FDA release from Ac/PBE-Dex 35% NPs. Cells were incubated with LPS 1 µg/ml to get the ON-state (marked green). After the addition of the particles, the release of DC-FDA was measured. To induce the OFF-system, prednisolone was added to shift the pH to pH 7,4 and the measurement was continued (marked red). Experiments have been conducted once (n = 1) with three technical replicates.

Abstract

This thesis examined the potential of nanoparticles (NPs) to revolutionize the treatment of rheumatoid arthritis (RA), a prevalent autoimmune disease requiring sustained therapy. By encapsulating bioactive agents, NPs enable targeted drug delivery that maintains therapeutic efficacy without necessitating increased drug concentrations or dosage frequency. The aim was to monitor model drug release in the cell environment during inflammation. A drug delivery system (DDS) was developed using model drug loaded acetalated dextran (Ac-Dex) and phenylboronic pinacol ester conjugated to acetalated dextran (Ac/PBE-Dex) NPs and involving macrophages in an inflammatory environment triggered by bacterial lipopolysaccharide (LPS). Using prednisolone to test the accuracy of the NPs, the study examined changes in fluorescence intensity (FI) to measure drug release effectiveness. The research process included characterizing the probes and NPs, and conducting cell studies for titration, cytotoxicity, and ON/OFF-system testing.

The sizes of the NPs increased in lower pH environment meaning that aggregation or swelling occurred. The significant decrease in PDI at lower pH demonstrated the uniformity of Ac-Dex NPs whereas an increase occurred with the Ac/PBE-Dex NPs. It was hypothesized that since those particles actually consisted of stabilized dextran, they were more stable and could be used as a reference in testing the DDS. The titration assays with 2’,7’-dichlorofluorescein diacetate (DC-FDA) did not reveal significant differences across varying LPS concentrations. This identical outcome, irrespective of LPS dosage, suggests a potential maximum threshold in the cellular response, beyond which no additional reaction was triggered. Both tested prednisolone concentrations significantly reduced the FI in LPS-stimulated cells, affirming its potency as a synthetic glucocorticoid that effectively mitigates inflammation. These results imply that prednisolone, regardless of the dosage, can effectively modulate the cellular response induced by LPS stimulation, likely through its interference with inflammation-related cellular pathways and gene expression.

Interleukin-6 (IL-6) levels were found to be higher in LPS samples incubated for three hours compared to those incubated for one hour, suggesting a time-dependent response in IL-6 production. Despite the lack of observable impact of prednisolone on IL-6 production, likely due to insufficient incubation time, its effect could still be detected in fluorescence intensity assays. A comprehensive assessment of the NPs biocompatibility was conducted, revealing that all NP samples maintained a cell viability level at or above the critical 70% threshold, indicating good biocompatibility. This outcome supports the potential of these NPs as a viable DDS for RA treatment, as the NPs, their cargo, and degradation products did not seem to exhibit notable cytotoxicity.

Despite various adjustments to the ON/OFF-system, no significant effects on cell activity were observed. These findings suggest that the proposed model using DC-FDA to track drug release lacked sufficient specificity and reproducibility, as differences in FI were statistically insignificant, and the cells could not be consistently deactivated. Further investigation is needed to fully ascertain the potential of the proposed DDS. Despite these challenges, the research offers valuable insights into the behaviour of NPs in an inflammatory environment, opening the door to potential advancements in targeted drug delivery for RA treatment.

Annotatsioon

Käesolev magistritöö uuris nanoosakeste kasutamist levinud autoimmuunhaiguse reumatoidartriidi ravis. Nanoosakesed võimaldavad bioaktiivseid aineid kapseldades sihipärast ravimite edastamist ning tagavad terapeutilise efektiivsuse ilma ravimi kontsentratsiooni või annustamissagedust suurendamata. Kasutades atsetaalitud dekstraani ja atsetaalitud dekstraani külge konjugeeritud fenüülboorpinakooli estri nanoosakesi ning kaasates makrofaage bakteriaalse lipopolüsahhariidi (LPS) esilekutsutud põletikutaolises keskkonnas loodi põletikuspetsiifiline ravimi edastamise süsteem. Rakkude puhkeoleku taastamiseks kasutati põletikuvähendava toimega glükokortikoidi prednisolooni ning järgnenud reaktsioone uuriti läbi fluorestsentsi mõõtmise, et tuvastada ravimi vabanemise efektiivsus. Töö hõlmas fluorestsentsete värvide ja nanoosakeste iseloomustamist ning rakkude uuringuid kasutatud ainete optimaalsete kontsentratsioonide määramiseks, tsütotoksilisuse ja nn sisse/välja-süsteemi testimiseks.

Nanoosakeste suurused kasvasid happelisemas keskkonnas, mis viitab agregatsioonile või paisumisele. Polüdisperssuse indeksi oluline vähenemine happelises pH-s näitas atsetaalitud dekstraani nanoosakeste ühtlasemat suurusjaotuvust, samas kui teiste osakeste puhul toimus suurenemine. Oletati, et kuna need osakesed koosnesid tegelikult stabiliseeritud dekstraanist, olid need stabiilsemad ja neid võis kasutada sisse/välja-süsteemi testimisel võrdluseks. Fluorestsentse värvi tiitrimise katsetes ei paljastunud märkimisväärseid erinevusi erinevate LPS kontsentratsioonide vahel, mis viitab potentsiaalsele maksimaalsele lävendile rakulises reaktsioonis sõltumata LPS doosist. Mõlemad testitud prednisolooni kontsentratsioonid vähendasid oluliselt fluorestsentsi stimuleeritud rakkudes, kinnitades selle tõhusust põletiku vähendamisel. Need tulemused viitavad sellele, et prednisoloon suudab olenemata annusest tõhusalt modifitseerida stimulatsioonist tingitud rakulist vastust, tõenäoliselt sekkudes põletikuga seotud raku signaaliradadesse ja geeniekspressiooni.

Tsütokiini interleukiin-6 tasemed olid kõrgemad prednisolooniga stimuleeritud rakuproovides, mis olid inkubeeritud kolm tundi, võrreldes nendega, mis olid inkubeeritud ühe tunni demonstreerides ajast sõltuvale vastusele IL-6 tootmises. Vaatamata prednisolooni mõju puudumisele IL-6 tootmisele, tõenäoliselt ebapiisava inkubatsiooniaja tõttu, võis selle mõju siiski tuvastada fluorestsentsi intensiivsuses. Metabolismil põhineva elulevuse katsetega näidati nanoosakeste bioloogilist sobivust, kus kõik testitud nanoosakeste kontsentratsioonid säilitasid raku elujõulisuse taseme kriitilisel 70% lävendil või sellest kõrgemal, viidates heale bioloogilisele sobivusele. See tulemus toetab testitud nanoosakeste potentsiaali RA raviks sobiva ravimi edastamise süteemis, kuna neil ei olnud tsütotoksilist mõju.

Hoolimata mitmesugustest kohandustest ravimi edastamise süsteemis, ei täheldatud märkimisväärset erinevust mudelravimi vabanemisel. Tulemused viitavad sellele, et pakutud mudel, mis kasutas fluorestsentsi mudelravimi vabanemise jälgimiseks, ei olnud piisavalt spetsiifiline ja reprodutseeritav, kuna mõõdetud erinevused olid statistiliselt ebaolulised ja rakke ei saanud järjekindlalt välja lülitada. Vajalik on edasine uurimine, et kindlaks teha pakutud süsteemi efektiivsus. Vaatamata töös esinenud väljakutsetest demonstreeriti nanoosakeste käitumist põletikulises keskkonnas ning tehti paljulubavad edusammud RA raviks sihitud ravimite kohaletoimetamisel.

Acknowledgments

I am extremely grateful to have been surrounded by so many talented and supported individuals during my writing process. My sincere gratitude and appreciation go to my two supervisors Dr. Alexandra Stubelius and Dr. Kaja Kasemets for their support and guidance throughout my thesis journey. Their expert advice, valuable feedback, and insightful comments have been instrumental in shaping my work and pushing me towards excellence.

I would like to acknowledge PhD student Loise Råberg for helping me with cell studies, Dr. Gizem Erensoy for providing me with chemical knowledge and Endri Bardhi for the synthesis of the NPs. I extend my heartfelt thanks to all the members of our lab group and department at Chalmers who graciously shared their time and expertise with me, enabling me to gather valuable data for my study. Special thanks go to Dr. Anne Kahru for giving me general guidance in the world of science.

Finally, I am deeply indebted to my family and close ones who had my back and whose support and encouragement contributed to the progress and completion of this thesis.

References

[1] D. Furman *et al.*, ‘Chronic inflammation in the etiology of disease across the life span’, *Nat Med*, vol. 25, no. 12, pp. 1822–1832, Dec. 2019, doi: 10.1038/S41591-019-0675-0.

[2] A. K. Dhingra and B. Chopra, ‘Inflammation as a therapeutic target for various deadly disorders: A review’, *Curr Drug Targets*, vol. 21, no. 6, pp. 582–588, Dec. 2019, doi: 10.2174/1389450120666191204154115.

[3] World Health Organization, ‘The global burden of disease: 2004 update’, 2008.

[4] I. B. Mcinnes and G. Schett, ‘The pathogenesis of rheumatoid arthritis’, *N Engl J Med*, vol. 365, pp. 2205–2219, 2011, doi: 10.1056/NEJMra1004965.

[5] G. R. Burmester and J. E. Pope, ‘Novel treatment strategies in rheumatoid arthritis’, *The Lancet*, vol. 389, no. 10086, pp. 2338–2348, Jun. 2017, doi: 10.1016/S0140-6736(17)31491-5.

[6] C. T. N. Pham, ‘Nanotherapeutic approaches for the treatment of rheumatoid arthritis’, *WIREs Nanomedicine and Nanobiotechnology*, vol. 3, pp. 607–619, 2011, doi: 10.1002/wnan.157.

[7] E. A. Littlejohn and S. U. Monrad, ‘Early diagnosis and treatment of rheumatoid arthritis’, *Primary Care: Clinics in Office Practice*, vol. 45, no. 2, pp. 237–255, Jun. 2018, doi: 10.1016/J.POP.2018.02.010.

[8] A. F. Radu and S. G. Bungau, ‘Management of rheumatoid arthritis: An overview’, *Cells*, vol. 10, no. 11, p. 2857, Oct. 2021, doi: 10.3390/CELLS10112857.

[9] W. Kurowska, E. H. Kuca-Warnawin, A. Radzikowska, and W. Maslinski, ‘The role of anti-citrullinated protein antibodies (ACPA) in the pathogenesis of rheumatoid arthritis’, *Central European Journal of Immunology*, vol. 42, no. 4, pp. 390–398, 2017, doi: 10.5114/CEJI.2017.72807.

[10] K. A. Theis, A. Steinweg, C. G. Helmick, E. Courtney-Long, J. A. Bolen, and R. Lee, ‘Which one? What kind? How many? Types, causes, and prevalence of disability among U.S. adults’, *Disabil Health J*, vol. 12, no. 3, pp. 411–421, Jul. 2019, doi: 10.1016/J.DHJO.2019.03.001.

[11] S. F. Lanes *et al.*, ‘Resource utilization and cost of care for rheumatoid arthritis and osteoarthritis in a managed care setting. The importance of drug and surgery costs’, *Arthritis Rheum*, vol. 40, no. 8, pp. 1475–1481, Aug. 1997, doi: 10.1002/ART.1780400816.

[12] D. Giannini, M. Antonucci, F. Petrelli, S. Bilia, A. Alunno, and I. Puxeddu, ‘One year in review 2020: Pathogenesis of rheumatoid arthritis’, *Clin Exp Rheumatol*, vol. 38, no. 3, pp. 387–397, May 2020, doi: 10.55563/clinexprheumatol/3uj1ng.

[13] N. Hannemann, F. Apparailly, and G. Courties, ‘Synovial macrophages: from ordinary eaters to extraordinary multitaskers’, *Trends Immunol*, vol. 42, no. 5, pp. 368–371, May 2021, doi: 10.1016/j.it.2021.03.002.

[14] Y. Itoh, ‘Metalloproteinases in rheumatoid arthritis: Potential therapeutic targets to improve current therapies’, *Prog Mol Biol Transl Sci*, vol. 148, pp. 327–338, Jan. 2017, doi: 10.1016/BS.PMBTS.2017.03.002.

[15] B. Bartok and G. S. Firestein, ‘Fibroblast-like synoviocytes: Key effector cells in rheumatoid arthritis’, *Immunol Rev*, vol. 233, no. 1, pp. 233–255, Jan. 2010, doi: 10.1111/J.0105-2896.2009.00859.X.

[16] Q. Guo, Y. Wang, D. Xu, J. Nossent, N. J. Pavlos, and J. Xu, ‘Rheumatoid arthritis: Pathological mechanisms and modern pharmacologic therapies’, *Bone Research 2018 6:1*, vol. 6, no. 1, pp. 1–14, Apr. 2018, doi: 10.1038/s41413-018-0016-9.

[17] S. K. Lundy, S. Sarkar, L. A. Tesmer, and D. A. Fox, ‘Cells of the synovium in rheumatoid arthritis. T lymphocytes’, *Arthritis Res Ther*, vol. 9, no. 1, pp. 1–11, Feb. 2007, doi: 10.1186/AR2107/TABLES/1.

[18] A. R. Phull, B. Nasir, I. ul Haq, and S. J. Kim, ‘Oxidative stress, consequences and ROS mediated cellular signaling in rheumatoid arthritis’, *Chem Biol Interact*, vol. 281, pp. 121–136, Feb. 2018, doi: 10.1016/J.CBI.2017.12.024.

[19] V. M. Holers and N. K. Banda, ‘Complement in the initiation and evolution of rheumatoid arthritis’, *Front Immunol*, vol. 9, no. MAY, p. 1057, May 2018, doi: 10.3389/FIMMU.2018.01057/BIBTEX.

[20] E. M. Paleolog, ‘Angiogenesis in rheumatoid arthritis’, *Arthritis Res*, vol. 4, no. 3, pp. S81–S90, May 2002, doi: 10.1186/AR575/TABLES/2.

[21] J. I. Saldana, ‘Macrophages | British Society for Immunology’. https://www.immunology.org/public-information/bitesized-immunology/cells/macrophages (accessed Apr. 16, 2023).

[22] F. O. Martinez and S. Gordon, ‘The M1 and M2 paradigm of macrophage activation: Time for reassessment’, *F1000Prime Rep*, vol. 6, Mar. 2014, doi: 10.12703/P6-13.

[23] A. Sica and A. Mantovani, ‘Macrophage plasticity and polarization: In vivo veritas’, *J Clin Invest*, vol. 122, no. 3, pp. 787–795, Mar. 2012, doi: 10.1172/JCI59643.

[24] P. J. Murray *et al.*, ‘Macrophage activation and polarization: Nomenclature and experimental guidelines’, *Immunity*, vol. 41, no. 1, pp. 14–20, Jul. 2014, doi: 10.1016/J.IMMUNI.2014.06.008.

[25] R. W. Kinne, B. Stuhlmüller, and G. R. Burmester, ‘Cells of the synovium in rheumatoid arthritis. Macrophages’, *Arthritis Res Ther*, vol. 9, no. 6, pp. 1–16, Dec. 2007, doi: 10.1186/AR2333/FIGURES/3.

[26] G. Dennis *et al.*, ‘Synovial phenotypes in rheumatoid arthritis correlate with response to biologic therapeutics’, *Arthritis Res Ther*, vol. 16, no. 2, pp. 1–18, Apr. 2014, doi: 10.1186/AR4555/TABLES/1.

[27] A. Kennedy, U. Fearon, D. J. Veale, and C. Godson, ‘Macrophages in synovial inflammation’, *Front Immunol*, vol. 2, no. OCT, p. 52, Oct. 2011, doi: 10.3389/FIMMU.2011.00052/BIBTEX.

[28] J. L. Davignon *et al.*, ‘Targeting monocytes/macrophages in the treatment of rheumatoid arthritis’, *Rheumatology*, vol. 52, no. 4, pp. 590–598, Apr. 2013, doi: 10.1093/RHEUMATOLOGY/KES304.

[29] M. M. J. Herenius *et al.*, ‘Monocyte migration to the synovium in rheumatoid arthritis patients treated with adalimumab’, *Ann Rheum Dis*, vol. 70, no. 6, pp. 1160–1162, Jun. 2011, doi: 10.1136/ARD.2010.141549.

[30] M. A. Boutet *et al.*, ‘Novel insights into macrophage diversity in rheumatoid arthritis synovium’, *Autoimmun Rev*, vol. 20, no. 3, p. 102758, Mar. 2021, doi: 10.1016/J.AUTREV.2021.102758.

[31] M. Biniecka *et al.*, ‘Dysregulated bioenergetics: A key regulator of joint inflammation’, *Ann Rheum Dis*, vol. 75, no. 12, pp. 2192–2200, Dec. 2016, doi: 10.1136/ANNRHEUMDIS-2015-208476.

[32] G. M. Tannahill *et al.*, 'Succinate is an inflammatory signal that induces IL-1β through HIF-1α', *Nature*, vol. 496, no. 7444, pp. 238–242, Mar. 2013, doi: 10.1038/nature11986.

[33] T. Cramer *et al.*, 'HIF-1α is essential for myeloid cell-mediated inflammation', *Cell*, vol. 112, no. 5, pp. 645–657, Mar. 2003, doi: 10.1016/S0092-8674(03)00154-5.

[34] A. V. Misharin *et al.*, 'Nonclassical Ly6C- monocytes drive the development of inflammatory arthritis in mice', *Cell Rep*, vol. 9, no. 2, pp. 591–604, Oct. 2014, doi: 10.1016/j.celrep.2014.09.032.

[35] I. A. Udalova, A. Mantovani, and M. Feldmann, 'Macrophage heterogeneity in the context of rheumatoid arthritis', *Nature Reviews Rheumatology 2016 12:8*, vol. 12, no. 8, pp. 472–485, Jul. 2016, doi: 10.1038/nrrheum.2016.91.

[36] K. M. Peters, K. Koberg, T. Rosendahl, B. Klosterhalfen, A. Straub, and G. Zwadlo-Klarwasser, 'Macrophage reactions in septic arthritis', *Arch Orthop Trauma Surg*, vol. 115, no. 6, pp. 347–350, 1996, doi: 10.1007/BF00420330/METRICS.

[37] L. Yeo *et al.*, 'Expression of chemokines CXCL4 and CXCL7 by synovial macrophages defines an early stage of rheumatoid arthritis', *Ann Rheum Dis*, vol. 75, no. 4, pp. 763–771, Apr. 2016, doi: 10.1136/ANNRHEUMDIS-2014-206921.

[38] A. Cauli, G. Yanni, and G. S. Panayi, 'Interleukin-1, interleukin-1 receptor antagonist and macrophage populations in rheumatoid arthritis synovial membrane.', *Rheumatology*, vol. 36, no. 9, pp. 935–940, Sep. 1997, doi: 10.1093/RHEUMATOLOGY/36.9.935.

[39] T. Vogl *et al.*, 'Alarmin S100A8/S100A9 as a biomarker for molecular imaging of local inflammatory activity', *Nat Commun*, vol. 5, no. 1, pp. 1–12, Aug. 2014, doi: 10.1038/ncomms5593.

[40] L. De Rycke *et al.*, 'Differential expression and response to anti-TNFα treatment of infiltrating versus resident tissue macrophage subsets in autoimmune arthritis', *J Pathol*, vol. 206, no. 1, pp. 17–27, May 2005, doi: 10.1002/PATH.1758.

[41] D. Aletaha *et al.*, '2010 Rheumatoid arthritis classification criteria: An American College of Rheumatology/European League Against Rheumatism collaborative initiative', *Arthritis Rheum*, vol. 62, no. 9, pp. 2569–2581, Sep. 2010, doi: 10.1002/ART.27584.

[42] J. A. Singh *et al.*, '2015 American College of Rheumatology guideline for the treatment of rheumatoid arthritis', *Arthritis and Rheumatology*, vol. 68, no. 1, pp. 1–26, Jan. 2016, doi: 10.1002/ART.39480/ABSTRACT.

[43] M. Del Grossi Moura, L. C. Lopes, M. T. Silva, S. Barberato-Filho, R. H. L. Motta, and C. De Cássia Bergamaschi, 'Use of steroid and nonsteroidal anti-inflammatories in the treatment of rheumatoid arthritis: Systematic review protocol', *Medicine (United States)*, vol. 97, no. 41, Oct. 2018, doi: 10.1097/MD.0000000000012658.

[44] J. S. Smolen *et al.*, 'EULAR recommendations for the management of rheumatoid arthritis with synthetic and biological disease-modifying antirheumatic drugs: 2019 update', *Ann Rheum Dis*, vol. 79, no. 6, pp. 685–699, Jun. 2020, doi: 10.1136/ANNRHEUMDIS-2019-216655.

[45] S. L. Whittle *et al.*, 'Multinational evidence-based recommendations for pain management by pharmacotherapy in inflammatory arthritis: integrating systematic literature research and expert opinion of a broad panel of rheumatologists in the 3e Initiative', *Rheumatology*, vol. 51, no. 8, pp. 1416–1425, Aug. 2012, doi: 10.1093/RHEUMATOLOGY/KES032.

[46] M. C. Hochberg, ‘New directions in symptomatic therapy for patients with osteoarthritis and rheumatoid arthritis’, *Semin Arthritis Rheum*, vol. 32, no. 3, pp. 4–14, Dec. 2002, doi: 10.1053/SARH.2002.37215.

[47] L. J. Crofford, ‘Use of NSAIDs in treating patients with arthritis’, *Arthritis Res Ther*, vol. 15, no. SUPPL 3, pp. 1–10, Jul. 2013, doi: 10.1186/AR4174/TABLES/4.

[48] L. R. Ballou, R. M. Botting, S. Goorha, J. Zhang, and J. R. Vane, ‘Nociception in cyclooxygenase isozyme-deficient mice’, *Proc Natl Acad Sci U S A*, vol. 97, no. 18, pp. 10272–10276, Aug. 2000, doi: 10.1073/PNAS.180319297.

[49] D. C. Brater, C. Harris, J. S. Redfern, and B. J. Gertz, ‘Renal effects of COX-2-selective inhibitors’, *Am J Nephrol*, vol. 21, no. 1, pp. 1–15, 2001, doi: 10.1159/000046212.

[50] S. Trelle *et al.*, ‘Cardiovascular safety of non-steroidal anti-inflammatory drugs: Network meta-analysis’, *BMJ*, vol. 342, no. 7789, p. 154, Jan. 2011, doi: 10.1136/BMJ.C7086.

[51] L. A. García Rodríguez, S. Tacconelli, and P. Patrignani, ‘Role of dose potency in the prediction of risk of myocardial infarction associated with nonsteroidal anti-inflammatory drugs in the general population’, *J Am Coll Cardiol*, vol. 52, no. 20, pp. 1628–1636, Nov. 2008, doi: 10.1016/J.JACC.2008.08.041.

[52] F. Buttgereit, ‘Do the treatment with glucocorticoids and/or the disease itself drive the impairment in glucose metabolism in patients with rheumatoid arthritis?’, *Ann Rheum Dis*, vol. 70, no. 11, pp. 1881–1883, Nov. 2011, doi: 10.1136/ANNRHEUMDIS-2011-200388.

[53] R. B. M. Landewé *et al.*, ‘COBRA combination therapy in patients with early rheumatoid arthritis: Long-term structural benefits of a brief intervention’, *Arthritis Rheum*, vol. 46, no. 2, pp. 347–356, 2002, doi: 10.1002/ART.10083.

[54] J. N. Hoes *et al.*, ‘Glucose tolerance, insulin sensitivity and β-cell function in patients with rheumatoid arthritis treated with or without low-to-medium dose glucocorticoids’, *Ann Rheum Dis*, vol. 70, no. 11, pp. 1887–1894, Nov. 2011, doi: 10.1136/ARD.2011.151464.

[55] J. Bullock *et al.*, ‘Rheumatoid arthritis: A brief overview of the treatment’, *Medical Principles and Practice*, vol. 27, no. 6, pp. 501–507, Mar. 2018, doi: 10.1159/000493390.

[56] L. Fraenkel *et al.*, ‘2021 American College of Rheumatology guideline for the treatment of rheumatoid arthritis’, *Arthritis Rheumatol*, vol. 73, no. 7, pp. 1108–1123, Jul. 2021, doi: 10.1002/ART.41752.

[57] S. Xiao, Y. Tang, Z. Lv, Y. Lin, and L. Chen, ‘Nanomedicine - advantages for their use in rheumatoid arthritis theranostics’, *J Control Release*, vol. 316, pp. 302–316, Dec. 2019, doi: 10.1016/J.JCONREL.2019.11.008.

[58] S. K. Nitta and K. Numata, ‘Biopolymer-based nanoparticles for drug/gene delivery and tissue engineering’, *Int J Mol Sci*, vol. 14, no. 1, p. 1629, 2013, doi: 10.3390/IJMS14011629.

[59] Q. Wang, X. Qin, J. Fang, and X. Sun, ‘Nanomedicines for the treatment of rheumatoid arthritis: State of art and potential therapeutic strategies’, *Acta Pharm Sin B*, vol. 11, no. 5, p. 1158, May 2021, doi: 10.1016/J.APSB.2021.03.013.

[60] M. J. Ansari, ‘Factors affecting preparation and properties of nanoparticles by nanoprecipitation method’, *Indo American Journal of Pharmaceutical Sciences*, vol. 4, no. 12, pp. 4854–4858, 2017, doi: 10.5281/zenodo.1134425.

[61] S. Salatin, J. Barar, M. Barzegar-Jalali, K. Adibkia, F. Kiafar, and M. Jelvehgari, ‘Development of a nanoprecipitation method for the entrapment of a very water soluble drug into Eudragit RL nanoparticles’, *Res Pharm Sci*, vol. 12, no. 1, pp. 1–14, Feb. 2017, doi: 10.4103/1735-5362.199041.

[62] J. Y. Zhang *et al.*, ‘Preparation of amorphous cefuroxime axetil nanoparticles by controlled nanoprecipitation method without surfactants’, *Int J Pharm*, vol. 323, no. 1–2, pp. 153–160, Oct. 2006, doi: 10.1016/J.IJPHARM.2006.05.048.

[63] J. Cheng *et al.*, ‘Formulation of functionalized PLGA-PEG nanoparticles for in vivo targeted drug delivery’, *Biomaterials*, vol. 28, no. 5, pp. 869–876, Feb. 2007, doi: 10.1016/J.BIOMATERIALS.2006.09.047.

[64] W. Huang and C. Zhang, ‘Tuning the size of poly(lactic-co-glycolic acid) (PLGA) nanoparticles fabricated by nanoprecipitation’, *Biotechnol J*, vol. 13, no. 1, Jan. 2018, doi: 10.1002/BIOT.201700203.

[65] K. S. Yadav and K. K. Sawant, ‘Modified nanoprecipitation method for preparation of cytarabine-loaded PLGA nanoparticles’, *AAPS PharmSciTech*, vol. 11, no. 3, pp. 1456–1465, 2010, doi: 10.1208/s12249-010-9519-4.

[66] P. Prasher *et al.*, ‘Versatility of acetalated dextran in nanocarriers targeting respiratory diseases’, *Mater Lett*, vol. 323, p. 132600, Sep. 2022, doi: 10.1016/J.MATLET.2022.132600.

[67] E. M. Bachelder, T. T. Beaudette, K. E. Broaders, J. Dashe, and J. M. J. Fréchet, ‘Acetal-derivatized dextran: An acid-responsive biodegradable material for therapeutic applications’, *J Am Chem Soc*, vol. 130, no. 32, pp. 10494–10495, Aug. 2008, doi: 10.1021/JA803947S/SUPPL_FILE/JA803947S-FILE003.PDF.

[68] R. Gannimani, P. Walvekar, V. R. Naidu, T. M. Aminabhavi, and T. Govender, ‘Acetal containing polymers as pH-responsive nano-drug delivery systems’, *Journal of Controlled Release*, vol. 328, pp. 736–761, Dec. 2020, doi: 10.1016/J.JCONREL.2020.09.044.

[69] R. Li *et al.*, ‘Acetalated dextran based nano-and microparticles: Synthesis, fabrication, and therapeutic applications’, *Chem. Commun*, vol. 57, p. 4212, 2021, doi: 10.1039/d1cc00811k.

[70] K. E. Broaders, J. A. Cohen, T. T. Beaudette, E. M. Bachelder, and J. M. J. Fréchet, ‘Acetalated dextran is a chemically and biologically tunable material for particulate immunotherapy’, *Proc Natl Acad Sci U S A*, vol. 106, no. 14, pp. 5497–5502, Apr. 2009, doi: 10.1073/PNAS.0901592106/ASSET/B1AFC088-CF92-4436-96FF-E49486CBCE85/ASSETS/GRAPHIC/ZPQ9990974490006.JPEG.

[71] A. Stubelius, S. Lee, and A. Almutairi, ‘The chemistry of boronic acids in nanomaterials for drug delivery’, *Acc Chem Res*, vol. 52, no. 11, pp. 3108–3119, 2019, doi: 10.1021/acs.accounts.9b00292.

[72] A. J. Manaster *et al.*, ‘Oxidation-sensitive dextran-based polymer with improved processability through stable boronic ester groups’, *ACS Appl Bio Mater*, vol. 2, no. 9, pp. 3755–3762, Sep. 2019, doi: 10.1021/ACSABM.9B00399.

[73] Y. Yang *et al.*, ‘Targeted silver nanoparticles for rheumatoid arthritis therapy via macrophage apoptosis and Re-polarization’, *Biomaterials*, vol. 264, p. 120390, Jan. 2021, doi: 10.1016/J.BIOMATERIALS.2020.120390.

[74] H. Kang *et al.*, ‘Size-dependent EPR effect of polymeric nanoparticles on tumor targeting’, *Adv Healthc Mater*, vol. 9, no. 1, p. 1901223, Jan. 2020, doi: 10.1002/ADHM.201901223.

[75] F. Canal, M. J. Vicent, G. Pasut, and O. Schiavon, ‘Relevance of folic acid/polymer ratio in targeted PEG–epirubicin conjugates’, *Journal of Controlled Release*, vol. 146, no. 3, pp. 388–399, Sep. 2010, doi: 10.1016/J.JCONREL.2010.05.027.

[76] N. Gaspar, G. Zambito, C. M. W. G. Löwik, and L. Mezzanotte, ‘Active nano-targeting of macrophages’, *Curr Pharm Des*, vol. 25, no. 17, pp. 1951–1961, Jul. 2019, doi: 10.2174/1381612825666190710114108.

[77] F. Salahpour Anarjan, ‘Active targeting drug delivery nanocarriers: Ligands’, *Nano-Structures & Nano-Objects*, vol. 19, p. 100370, Jul. 2019, doi: 10.1016/J.NANOSO.2019.100370.

[78] BioRender, ‘BioRender’, 2023. https://app.biorender.com/illustrations/6438055f61f5372fdd69ce92 (accessed Apr. 16, 2023).

[79] S. Behzadi *et al.*, ‘Cellular uptake of nanoparticles: Journey inside the cell’, *Chem Soc Rev*, vol. 46, no. 14, pp. 4218–4244, Jul. 2017, doi: 10.1039/C6CS00636A.

[80] S. Olsnes and K. Sandvig, ‘How protein toxins enter and kill cells.’, *Cancer Treat Res*, vol. 37, pp. 39–73, 1988, doi: 10.1007/978-1-4613-1083-9_4/COVER.

[81] B. Rotman and B. W. Papermaster, ‘Membrane properties of living mammalian cells as studied by enzymatic hydrolysis of fluorogenic esters’, *Med. Res. Council, Spec. Rept. Ser*, vol. 55, no. 1, pp. 134–141, 1966, doi: 10.1073/pnas.55.1.134.

[82] J. B. Grimm, L. M. Heckman, and L. D. Lavis, ‘The chemistry of small-molecule fluorogenic probes’, *Prog Mol Biol Transl Sci*, vol. 113, pp. 1–34, Jan. 2013, doi: 10.1016/B978-0-12-386932-6.00001-6.

[83] D. Wu and P. Yotnda, ‘Production and detection of reactive oxygen species (ROS) in cancers’, *J Vis Exp*, no. 57, p. 3357, 2011, doi: 10.3791/3357.

[84] H. Mayer, R. N. Tharanathan, and J. Weckesser, ‘6 Analysis of lipopolysaccharides of gram-negative bacteria’, *Methods in Microbiology*, vol. 18, no. C, pp. 157–207, Jan. 1985, doi: 10.1016/S0580-9517(08)70475-6.

[85] M. Muroi and K. ichi Tanamoto, ‘The polysaccharide portion plays an indispensable role in Salmonella lipopolysaccharide-induced activation of NF-κB through human toll-like receptor 4’, *Infect Immun*, vol. 70, no. 11, pp. 6043–6047, Nov. 2002, doi: 10.1128/IAI.70.11.6043-6047.2002/ASSET/44E3C7EC-5335-4876-A639-6ED0435533F1/ASSETS/GRAPHIC/II1120416004.JPEG.

[86] C. H. Lang, C. Silvis, N. Deshpande, G. Nystrom, and R. A. Frost, ‘Endotoxin stimulates in vivo expression of inflammatory cytokines tumor necrosis factor alpha, interleukin-1beta, -6, and high-mobility-group protein-1 in skeletal muscle.’, *Shock*, vol. 19, no. 6, pp. 538–546, 2003, doi: 10.1097/01.shk.0000055237.25446.80.

[87] BioLegend Inc, ‘Human IL-6 ELISA MAX^{TM} Deluxe Set’. [Online]. Available: www.biolegend.com/msds

[88] S. M. Moghimi, A. C. Hunter, and J. C. Murray, ‘Long-circulating and target-specific nanoparticles: theory to practice’, *Pharmacol Rev*, vol. 53, no. 2, pp. 283–318, 2001, Accessed: May 12, 2023. [Online]. Available: https://pubmed.ncbi.nlm.nih.gov/11356986/

[89] K. Chu *et al.*, ‘Nanoparticle drug loading as a design parameter to improve docetaxel pharmacokinetics and efficacy’, *Biomaterials*, vol. 34, no. 33, pp. 8424–8429, Nov. 2013, doi: 10.1016/j.biomaterials.2013.07.038.

[90] S. G. M. Ong, L. C. Ming, K. S. Lee, and K. H. Yuen, ‘Influence of the encapsulation efficiency and size of liposome on the oral bioavailability of griseofulvin-loaded liposomes’, *Pharmaceutics*, vol. 8, no. 3, Sep. 2016, doi: 10.3390/pharmaceutics8030025.

[91] J. M. Clarke, M. R. Gillings, N. Altavilla, and A. J. Beattie, ‘Potential problems with fluorescein diacetate assays of cell viability when testing natural products for antimicrobial activity’, *J Microbiol Methods*, vol. 46, no. 3, pp. 261–267, 2001, doi: 10.1016/S0167-7012(01)00285-8.

[92] N. Perrimon and A. P. McMahon, ‘Negative feedback mechanisms and their roles during pattern formation’, *Cell*, vol. 97, no. 1, pp. 13–16, Apr. 1999, doi: 10.1016/S0092-8674(00)80710-2.

[93] K. Ruckdeschel and K. Richter, ‘Lipopolysaccharide Desensitization of Macrophages Provides Protection against Yersinia enterocolitica-Induced Apoptosis’, *Infect Immun*, vol. 70, no. 9, p. 5259, Sep. 2002, doi: 10.1128/IAI.70.9.5259-5264.2002.

[94] M. Heimbürger, G. Lärfars, and J. Bratt, ‘Prednisolone inhibits cytokine-induced adhesive and cytotoxic interactions between endothelial cells and neutrophils in vitro’, *Clin Exp Immunol*, vol. 119, no. 3, p. 441, 2000, doi: 10.1046/J.1365-2249.2000.01165.X.

[95] National Cancer Institute, ‘Definition of prednisolone - NCI Drug Dictionary’. https://www.cancer.gov/publications/dictionaries/cancer-drug/def/prednisolone (accessed Apr. 16, 2023).

[96] K. Ulbrich, K. Holá, V. Šubr, A. Bakandritsos, J. Tuček, and R. Zbořil, ‘Targeted drug delivery with polymers and magnetic nanoparticles: Covalent and noncovalent approaches, release control, and clinical studies’, *Chem Rev*, vol. 116, no. 9, pp. 5338–5431, May 2016, doi: 10.1021/ACS.CHEMREV.5B00589.

[97] S. Pirmardvand Chegini, J. Varshosaz, and S. Taymouri, ‘Recent approaches for targeted drug delivery in rheumatoid arthritis diagnosis and treatment’, *Artif Cells Nanomed Biotechnol*, vol. 46, no. sup2, pp. 502–514, Nov. 2018, doi: 10.1080/21691401.2018.1460373.

Appendices

Appendix 1 Cell splitting protocol

Cell splitting was carried out every two to three days according to the following steps:

1) aspirate old media from the cell culture flask
2) wash cells with 10 ml of pre-warmed dPBS
3) aspirate dPBS
4) add 3 ml of trypsin to detach the cells from the flask surface and incubate for 5 minutes at 37 °C and 5 % CO_2. If cells are very confluent, increase the volume of trypsin and incubate as long as necessary
5) add 5-8 ml of DMEM complete medium to neutralize the trypsin and pipette cells up and down to disintegrate cell aggregates
6) transfer the cell suspension to a 15 ml tube and centrifuge for 5 minutes at 0,2 x g
7) discard the supernatant and add 1 ml of DMEM complete medium to the tube
8) mix 12 µl of Erythrosin B (a dye for staining nonviable cells) and 12 µl of the cell suspension in an Eppendorf tube
9) pipette 12 µl of the mix on both wells of a counting plate
10) count the cells in a counter and calculate the volume needed for splitting. The calculation formula: $cell\ volume = \frac{0{,}14 \cdot 10^6\ (cell\ concentration/ml) \cdot 10\ (ml)}{mean\ cell\ concentration/ml}$
11) add 10 ml of fresh complete medium to a new T75 cell culture flask and add the required volume of cells
12) incubate the cells at 37 °C and 5 % CO_2.

Non-exclusive Licence for Publication and Reproduction of Graduation Thesis

I, Laura Kaarma (date of birth: 08.09.1998)

1. grant Tallinn University of Technology free licence (non-exclusive licence) for my thesis “Controlling Drug Delivery through Nanoparticle and Macrophage Interactions: An Exploration of Inflammation Responsive Mechanisms” supervised by Alexandra Stubelius and Kaja Kasemets to be

1.1 reproduced for the purposes of preservation and electronic publication, incl. to be entered in the digital collection of TUT library until expiry of the term of copyright;

1.2 published via the web of Tallinn University of Technology, incl. to be entered in the digital collection of TTÜ library until expiry of the term of copyright.

2. I am aware that the author also retains the rights specified in clause 1.

3. I confirm that granting the non-exclusive licence does not infringe third persons’ intellectual property rights, the rights arising from the Personal Data Protection Act or rights arising from other legislation.

(signature)

(date)